

Design, Synthesis, and Biological Activity of Sulfonamide Analogues of Antofine and Cryptopleurine as Potent and Orally Active Antitumor Agents

Yongseok Kwon,^{†,||} Jayoung Song,^{‡,||} Honggu Lee,[†] Eun-Yeong Kim,[§] Kiho Lee,[§] Sang Kook Lee,^{*,‡} and Sanghee Kim^{*,†}

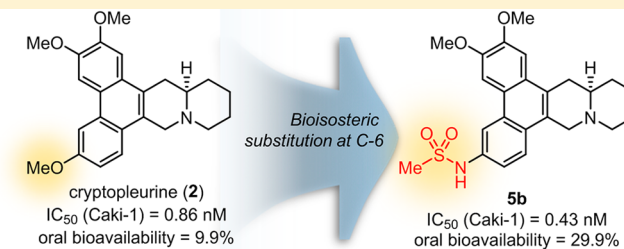
[†]Research Institute of Pharmaceutical Science, College of Pharmacy, Seoul National University, Seoul 151-742, Korea

[‡]Natural Products Research Institute, College of Pharmacy, Seoul National University, Seoul 151-742, Korea

[§]College of Pharmacy, Korea University, Sejong 339-700, Korea

Supporting Information

ABSTRACT: Due to their profound antiproliferative activity and unique mode of action, phenanthroindolizidine and phenanthroquinolizidine alkaloids, represented by antofine and cryptopleurine, have attracted attention recently as potential therapeutic agents. We have designed, synthesized, and evaluated the methanesulfonamide analogues of these natural alkaloids with the hope of improving their druglikeness. The analogues showed enhanced growth inhibition of human cancer cells compared with the parent natural products. In particular, a methanesulfonamide analogue of cryptopleurine (**5b**) exhibited improved bioavailability and significant antitumor activity, which suggests that **5b** is a promising new anticancer agent. Our studies suggest that the inhibition of cancer cell growth by **5b** is associated with the induction of G0/G1 cell cycle arrest via nicotinamide N-methyltransferase-dependent JNK activation in Caki-1 renal cancer cells. In addition, compound **5b** significantly inhibited the migration and invasion of Caki-1 cancer cells by modulating the p38 MAPK signaling pathway.



INTRODUCTION

Despite advances in modern drug discovery technologies, natural products are still an important source in the search for new therapeutics.¹ One plausible reason is that natural products have been evolutionarily selected and prevalidated by nature and thus display unique and highly useful biological activities.² Although many compounds derived from natural products exhibit potential pharmacological activity, structural modifications are often needed to render them effective clinical agents.

Phenanthroindolizidine and phenanthroquinolizidine alkaloids, represented by antofine (**1**, Figure 1) and cryptopleurine (**2**), respectively, are well-known for their profound antiproliferative activities.³ According to the National Cancer Institute's anticancer drug screen database, these compounds have significant activity, with IC₅₀ values in the nanomolar range against the ~60 cultured cancer cell lines tested.⁴ One of these classes of natural compounds, (*R*)-tylocrebrine (**3**), was once considered a potential candidate for an anticancer agent and was entered into clinical trials. However, tylocrebrine failed to gain approval due to irreversible central nervous system toxicity.⁵ In addition to the toxicity, these classes of alkaloids have additional drawbacks, including poor aqueous solubility and low metabolic stability.⁶

Recently, phenanthroindolizidine and phenanthroquinolizidine alkaloids have received renewed attention because of their unique mode of action, which differs from those of

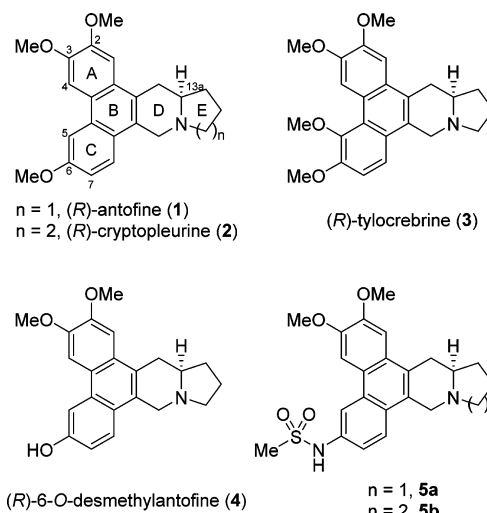


Figure 1. Chemical structures of compounds **1**–**5**.

currently available anticancer drugs.^{7–10} Although the precise molecular targets of these classes of compounds are still unclear, several mechanisms have been suggested, including the

Received: May 19, 2015

Published: September 22, 2015

inhibition of nucleic acid and protein synthesis,⁷ the inhibition of thymidylate synthase and dihydrofolate reductase,⁸ and the suppression of AP1-, CRE-, and NF- κ B-mediated transcription.⁹ Recent findings also suggest that these alkaloids elicit their biological activities through varying mechanisms of actions.¹⁰

Intensive structure–activity relationship (SAR) studies revealed several essential structural elements that are required for the cytotoxic activity of antofine and its related phenanthroindolizidine alkaloids.^{3,6,11} For example, the nonbonding electron pair on the nitrogen atom is important for significant activity. The pentacyclic system is also crucial for high cytotoxic activity. In the course of our SAR studies on the essential functional group requirement of the phenanthrene ring, we found that modest structural alterations to the C-6 methoxy group are seemingly allowed.^{6a} In addition, we recognized that the substituent at the C-6 position seems to function as a hydrogen bond donor because 6-O-desmethylantofine **4** exhibited greater cytotoxicity against cancer cells than the parent antofine. These findings prompted us to design analogues in which the C-6 methoxy group was replaced with other groups with hydrogen bond donor ability and higher polarity in the hope of overcoming the drawbacks of phenanthroindolizidine and phenanthroquinolizidine alkaloids.

Increasing the polarity via chemical modification is a promising strategy for improving the pharmacological and druglike properties of these alkaloids. However, only a few efforts have been made recently. K.-H. Lee and co-workers reported E-ring-hydroxylated antofine and cryptopleurine analogues. Some of these polar analogues exhibited notable cancer cell growth inhibition, but their inhibitory potency was much lower than that of the corresponding parent compounds.^{11b} In addition, E-ring-truncated phenanthroindolizidine analogues were also reported by S.-J. Lee and co-workers. One analogue with a hydroxyl group at the D-ring exhibited good bioavailability and good antiproliferative activity, with GI_{50} values of 0.02–0.06 μ M against human cancer cell lines.^{11c} In this regard, we have reported an antofine derivative with a hydroxymethyl substituent at C-13a. This polar analogue showed much better solubility in phosphate buffer (pH 7.4) than the parent compound (656 μ g/mL vs <1 μ g/mL).¹² The compound exhibited notable antiproliferative activity in both cell cultures and in vivo tumor xenograft models, but the in vitro antiproliferative activity of the compound was approximately 10-fold less compared with antofine. Therefore, we sought to further enhance the activity as well as the druglike properties of these alkaloids by chemically modifying the C-6 position.

We herein present novel polar analogues of antofine and cryptopleurine, **5a** and **5b** (Figure 1), which feature a methanesulfonamide group at the C-6 position of the phenanthrene ring. The antiproliferative activities of these analogues against various cancer cells were similar or even higher, with improved solubility and bioavailability, compared with the parent natural products. We further investigated the molecular mechanism of compound **5b** in Caki-1 human renal cancer cells and an in vivo xenograft model.

RESULTS AND DISCUSSION

Prediction of Physicochemical Properties. Our previous SAR studies suggested that the C-6 methoxy group could be replaced with other functional groups.^{6a} Among the various bioisosteres of the phenolic methoxy or hydroxyl group, we

selected the sulfonamide group because it can participate in hydrogen bonding and has similar pK_a values to that of the phenolic hydroxyl group. We anticipated that the polar, electron-withdrawing sulfonamide group would considerably alter the physicochemical properties of the parent natural products and, therefore, their pharmacokinetic properties. Our theoretical calculations on the designed methanesulfonamide analogues **5a** and **5b** indicated that the analogues have higher polar properties compared with the methoxy-group-containing natural products.¹³ The antofine analogue **5a** has a calculated AlogP value of 3.16 and a calculated polar surface area (PSA) of 68.6, whereas antofine has values of 4.24 and 30.1, respectively. The cryptopleurine analogue **5b** has an AlogP value of 3.62 and PSA of 68.6, whereas cryptopleurine has values of 5.59 and 30.1, respectively (Table 1). The calculated water solubilities of

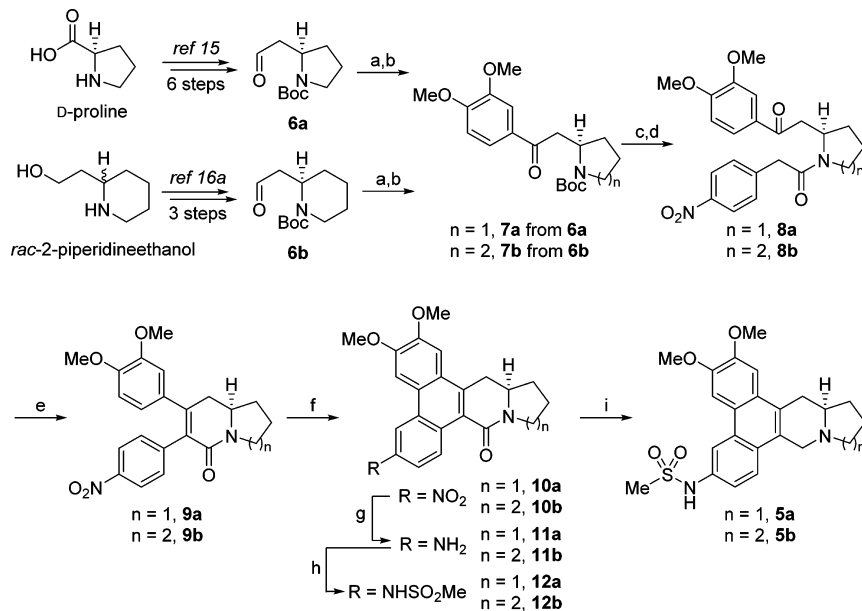
Table 1. Calculated Physicochemical Properties of Analogues **5a and **5b**^a**

compd	AlogP	PSA	logBB	solubility (μ g/mL)
5a	3.16	68.6	-0.262	0.649
5b	3.62	68.6	-0.121	0.277
antofine (1)	4.24	30.1	0.678	0.088
cryptopleurine (2)	5.59	30.1	0.819	0.036

^aAll physicochemical values were calculated using Biovia/ADME prediction software.

5a and **5b** were 0.649 and 0.277 μ g/mL, while those of antofine and cryptopleurine were 0.088 and 0.036 μ g/mL, respectively. The polar analogues **5a** and **5b** were also predicted to have better logBB values of -0.262 and -0.121, respectively, compared with 0.678 for antofine and 0.819 for cryptopleurine. Nevertheless, despite their increased polarity, the designed sulfonamide analogues are still in compliance with Lipinski's rule of five for druglikeness and oral bioavailability.¹⁴

Synthesis. The asymmetric synthesis of the designed analogues **5** was initiated by preparing the known aldehyde **6** in enantiomerically pure form. The (*R*)-N-Boc-2-(2-oxoethyl)-pyrrolidine (**6a**) was obtained from commercially available D-proline through a six-step sequence developed by Fürstner.¹⁵ The (*R*)-N-Boc-2-(2-oxoethyl)piperidine (**6b**) was obtained by resolution of *rac*-piperidineethanol by recrystallization of the salts formed with (1*R*)-10-camphorsulfonic acid, followed by Boc-protection and oxidation (98% ee).¹⁶ Treating the resulting aldehyde **6a** with arylmagnesium bromide, followed by oxidation, produced ketone **7a** at a 65% yield over two steps. Removal of the Boc protecting group and subsequent coupling with 4-nitrophenylacetic acid resulted in amide **8a** with a high overall yield (81%). This material was subjected to the basic intramolecular aldol condensation conditions to form an indolizidine ring system. A high yield of **9a** was obtained when K_2CO_3 was employed as a base in refluxing ethanol. Various reaction conditions were investigated to induce biaryl coupling for the construction of phenanthrene ring. We found that hypervalent iodine reagent phenyliodine(III) bis(trifluoroacetate) (PIFA)¹⁷ was the most effective in promoting the oxidative biaryl coupling of **9a** to give **10a** at 92% yield. The nitro group in **10a** was reduced to an amine group by hydrogenation over Pd/C to afford **11a**. Because this amine compound was unstable, it was immediately mesylated to form methanesulfonamide **12a** with a 58% yield over two steps. Finally, the amide group of **12a** was reduced with LiAlH₄ to form the desired antofine analogue **5a** at 66% yield. The

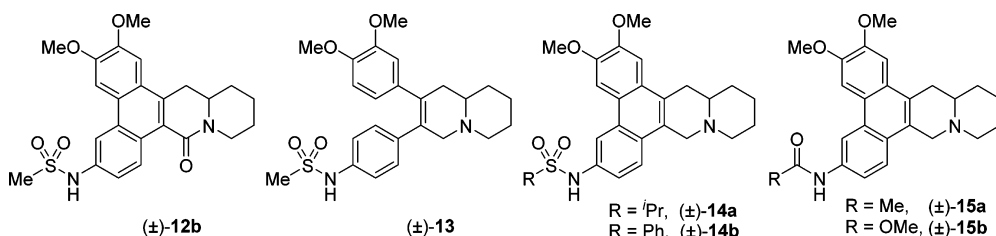
Scheme 1. Synthesis of Methanesulfonamide Analogue 5a and 5b^a

^aReaction conditions: (a) 3,4-dimethoxyphenylmagnesium bromide, THF, 0 °C; (b) PCC, 4 Å molecular sieves, CH₂Cl₂, 65% for 7a, 63% for 7b (over two steps); (c) TFA, CH₂Cl₂; (d) 4-nitrophenylacetic acid, EDCI, DMAP, CH₂Cl₂, 81% for 8a, 79% for 8b (over two steps); (e) K₂CO₃, EtOH, reflux, 82% for 9a, 86% for 9b; (f) PIFA, BF₃·OEt₂, CH₂Cl₂, -10 °C, 92% for 10a, 90% for 10b; (g) H₂, 10 wt % Pd/C, MeOH; (h) MeSO₂Cl, pyridine, CH₂Cl₂ 58% for 12a, 56% for 12b (over two steps); (i) LiAlH₄, THF, reflux, 66% for 5a, 62% for 5b.

Table 2. Antiproliferative Activities for Sulfonamide Analogues 5a and 5b

compd	IC ₅₀ (nM) ^a						
	A549 ^b	HCT-116 ^c	SNU-638 ^d	MDA-MB-231 ^e	SK-Hep-1 ^f	PC-3 ^g	Caki-1 ^h
5a	7.76 ± 0.56	3.49 ± 0.32	7.09 ± 0.46	4.59 ± 0.33	4.44 ± 0.52	8.31 ± 0.82	4.42 ± 0.21
5b	0.46 ± 0.03	0.48 ± 0.03	0.52 ± 0.02	0.38 ± 0.04	0.34 ± 0.05	0.75 ± 0.02	0.43 ± 0.02
antofine (1)	8.52 ± 0.80	6.03 ± 0.72	10.38 ± 0.56	6.04 ± 0.53	6.32 ± 0.62	12.34 ± 0.38	6.23 ± 0.33
cryptopleurine (2)	0.94 ± 0.12	1.04 ± 0.23	1.26 ± 0.16	0.89 ± 0.13	0.83 ± 0.17	2.55 ± 0.38	0.86 ± 0.13

^aAll values are the mean of at least three experiments. ^bHuman lung cancer cell line. ^cHuman colon cancer cell line. ^dHuman stomach cancer cell line. ^eHuman breast cancer cell line. ^fHuman liver cancer cell line. ^gHuman prostate cancer cell line. ^hHuman renal cancer cell line.

Table 3. Antiproliferative Activities for Analogue (\pm)-12b and (\pm)-13–15

entry	compd	IC ₅₀ (nM) ^a						
		A549 ^b	HCT-116 ^c	SNU-638 ^d	MDA-MB-231 ^e	SK-Hep-1 ^f	PC-3 ^g	Caki-1 ^h
1	(-)-5b	0.48 ± 0.05	0.53 ± 0.12	0.62 ± 0.10	0.46 ± 0.18	0.44 ± 0.13	1.21 ± 0.14	0.58 ± 0.09
2	(\pm)-5b	2.16 ± 0.32	2.01 ± 0.58	3.49 ± 0.62	2.08 ± 0.27	1.52 ± 0.40	4.74 ± 0.68	1.68 ± 0.31
3	(\pm)-12b	>100	>100	>100	>100	>100	>100	>100
4	(\pm)-13	>100	>100	>100	>100	>100	>100	>100
5	(\pm)-14a	56.03 ± 5.12	59.25 ± 12.38	68.32 ± 6.73	52.36 ± 4.29	49.23 ± 6.48	77.18 ± 13.63	37.73 ± 9.62
6	(\pm)-14b	99.93 ± 1.20	99.62 ± 0.98	>100	92.00 ± 6.32	99.48 ± 3.28	>100	99.45 ± 1.87
7	(\pm)-15a	4.60 ± 1.33	3.28 ± 1.10	6.59 ± 2.11	3.15 ± 1.56	1.64 ± 0.87	6.39 ± 1.97	2.19 ± 0.98
8	(\pm)-15b	6.21 ± 2.01	7.88 ± 2.32	9.08 ± 1.98	6.52 ± 1.72	2.50 ± 1.20	9.11 ± 2.77	5.78 ± 1.31

^aAll values are the mean of at least three experiments. ^bHuman lung cancer cell line. ^cHuman colon cancer cell line. ^dHuman stomach cancer cell line. ^eHuman breast cancer cell line. ^fHuman liver cancer cell line. ^gHuman prostate cancer cell line. ^hHuman renal cancer cell line.

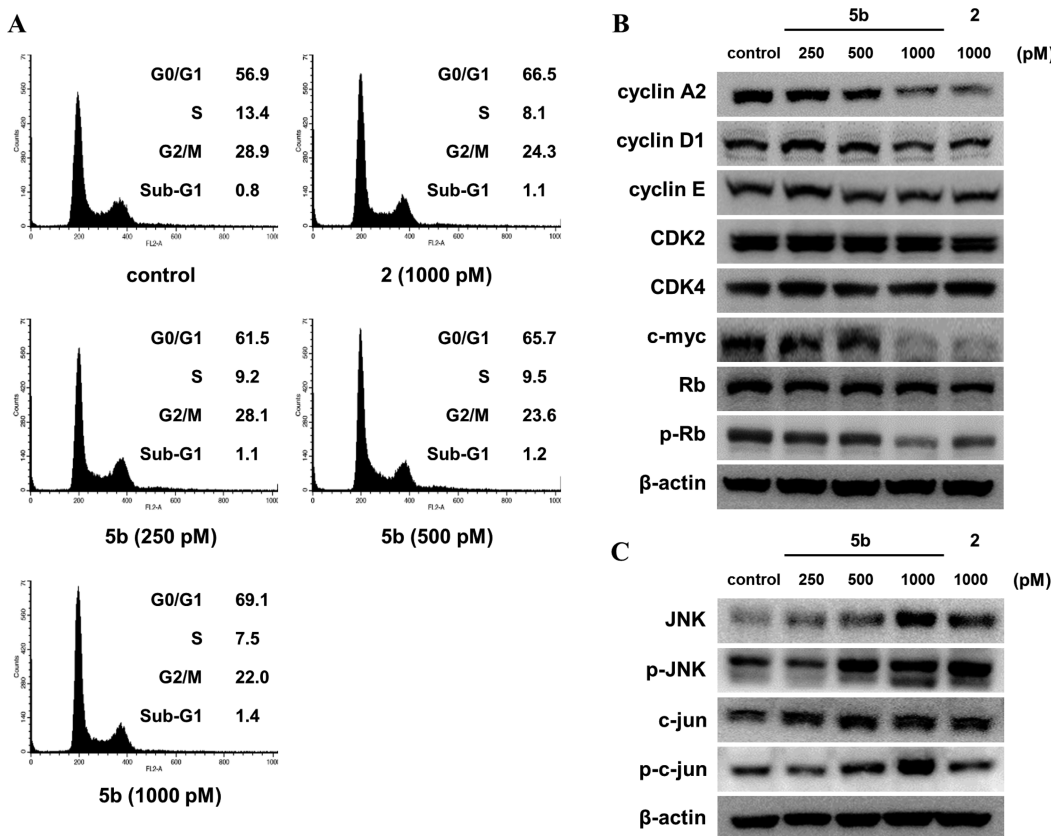


Figure 2. Effects of **5b** on cell cycle progression in Caki-1 cells. (A) Cell cycle analysis of Caki-1 cells. Cells were treated with the indicated concentrations of **5b** for 24 h. Both adherent and floating cells were collected, and DNA content was analyzed by flow cytometry. (B, C) Western blot analysis of Caki-1 cells. Cells were treated with the indicated concentrations of **5b** for 24 h. The parent compound, **2**, was used as the reference compound.

corresponding cryptopleurine analogue **5b** was synthesized with a similar overall yield in the same way but starting from **6b**. The structures of the final compounds were confirmed by spectroscopic methods, including IR, NMR, and mass spectroscopy.

Cancer Cell Growth-Inhibitory Effect of Sulfonamide Analogues. The growth-inhibitory activities of both methanesulfonamide analogues **5a** and **5b** were evaluated via SRB assays against various cancer cell lines. The IC₅₀ values for the analogues are summarized in Table 2. The antiproliferative activities of (*R*)-antofine and (*R*)-cryptopleurine were also evaluated for comparison. As reported in the literature,¹⁸ cryptopleurine showed very potent anticancer activity, with a 10- to 20-fold higher potency than antofine. Antofine analogue **5a** exhibited antiproliferative activity with IC₅₀ values in the low nanomolar range against the tested cancer cell lines. The potency of **5a** was slightly higher than that of antofine. The cryptopleurine analogue **5b** exhibited subnanomolar antiproliferative activity, with a more than 20-fold higher potency compared with antofine and its sulfonamide analogue **5a**. This analogue was approximately 2- to 3-fold more active than its parent natural product cryptopleurine. These results indicated that the methanesulfonamide group is amenable to substitute the C-6 methoxy group as a bioisostere with improved antiproliferative activity.¹⁹

Structure–Activity Relationship Study. After obtaining interesting results with C-6 methanesulfonamide analogues, several chemically modified analogues were investigated for the understanding of structure–activity relationships. The ana-

logues shown in Table 3 were prepared in racemic form by following a similar synthetic protocol to that described in Scheme 1.²⁰ Their antiproliferative activities were evaluated in comparison with **5b**, and the IC₅₀ values are listed in Table 3. The racemic form of **5b** was about 3- to 5-fold less active than its (−)-(*R*)-enantiomer (entry 1 vs 2). A similar decrease in activity was also observed in the racemic form of the sulfonamide analogue of antofine **5a** (data not shown). These results indicated that the stereochemistry at C-13a was very important for the antiproliferative activity of the sulfonamide analogues. In addition, the more than 2-fold decrease of activity in the racemate suggested that the (S)-enantiomer is not merely an inactive enantiomer but rather suppresses or interferes the antiproliferative activity of the (R)-enantiomer. The C-9 carbonyl analogue **12b** also showed dramatically decreased potency (entry 3), indicating the importance of a tertiary amine moiety for activity.^{3b,11g} The uncyclized C ring analogue **13** displayed a dramatic decrease in potency (entry 4). This result is in agreement with the previous SAR studies that established that the pentacyclic system is essential for high activity.^{3b}

Regarding the C-6 substituents, the bulkier sulfonamide group substantially decreased the potency; isopropylsulfonamide **14a** and benzenesulfonamide **14b** were less potent than the corresponding methanesulfonamide **5b** by ~20- to 50-fold (entries 5 and 6). These decreases in potency indicated that bulky groups are not well tolerated at 6-position of the phenanthrene ring. Methanesulfonamide **5b** was more potent than acetamide **15a** and methyl carbamate **15b** by ~2- to 4-fold (entry 2 vs entries 7 and 8). These findings suggested that the

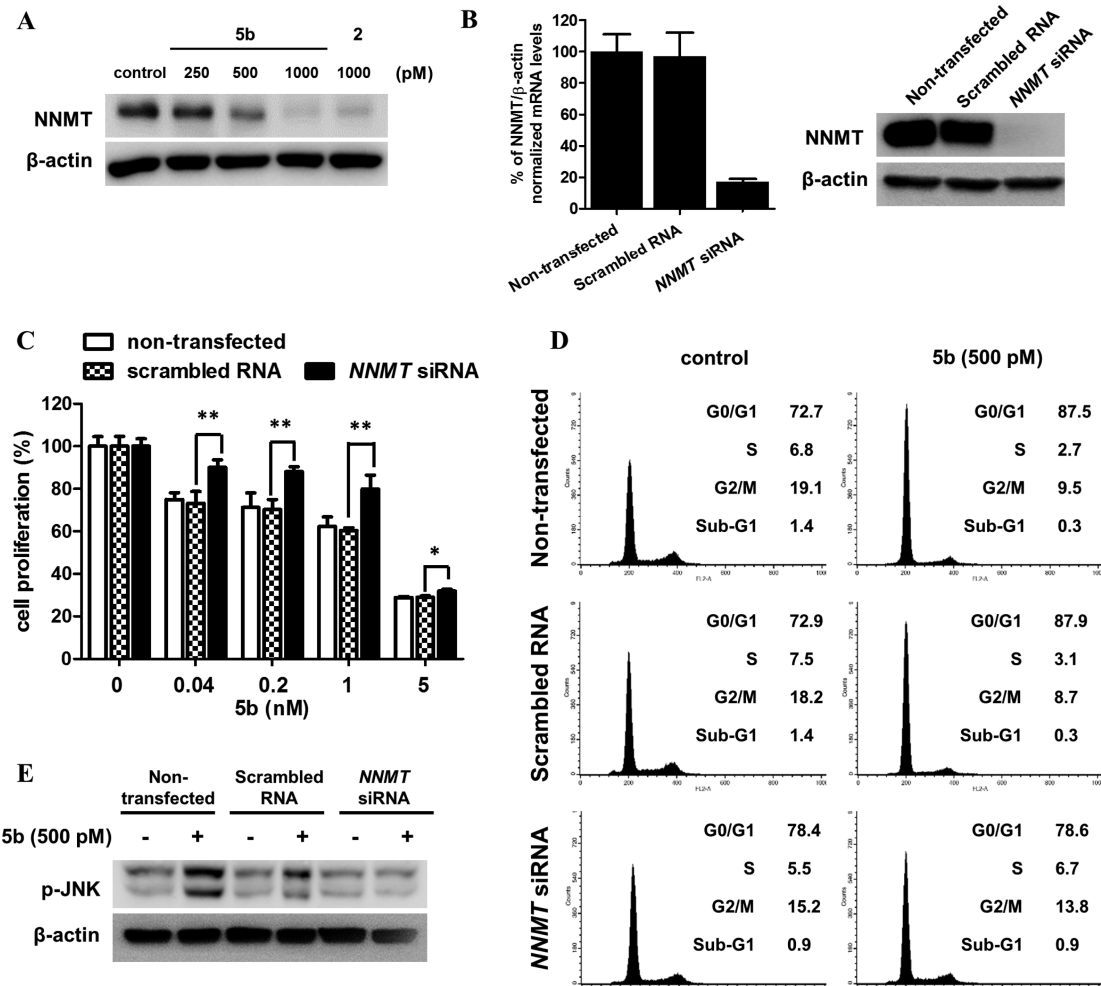


Figure 3. NNMT-dependent effects of **5b** on cell proliferation and cell cycle regulation. (A) Western blot analysis of Caki-1 cells. Cells were treated with the indicated concentrations of **5b** for 24 h. The parent compound, **2**, was used as the reference compound. (B) RNA interference experiments with Caki-1 cells. Caki-1 cells were not transfected or were transfected with scrambled siRNA or NNMT siRNA for 24 h. The levels of NNMT mRNA (left) and NNMT protein (right) expression are indicated. (C) Caki-1 cells were not transfected or were transfected with scrambled siRNA or NNMT siRNA for 24 h. The cells were seeded for 24 h and then treated with various concentrations of **5b** for 48 h. Cell proliferation was measured via SRB assay. The data are presented as the mean \pm SD. (*) $p < 0.05$, (**) $p < 0.01$ by *t*-test. (D) Caki-1 cells were not transfected or were transfected with scrambled siRNA or NNMT siRNA for 24 h. The cells were seeded for 24 h and then treated with or without 500 pM **5b** for 24 h. Both adherent and floating cells were collected, and DNA content was analyzed by flow cytometry. (E) Caki-1 cells were not transfected or were transfected with scrambled siRNA or NNMT siRNA for 24 h. The cells were seeded for 24 h and then treated with or without 500 pM **5b** for 24 h. The expression levels of the indicated proteins were analyzed by Western blot analysis.

acidity of C-6 amide proton might be important for high potency.

Regulation of Cell Cycle Progression. Given the high potency and enhanced antiproliferative activity of **5b** compared with the parent compound (*R*)-cryptopleurine (**2**), the detailed molecular mechanism of action of compound **5b** was evaluated in human Caki-1 renal cancer cells. Although the antiproliferative activity of **5b** was shown to be very potent against various cancer lines, we selected Caki-1 cells as a model cell line for these experiments. Caki-1 renal cell carcinoma is known to be highly metastatic and resistant to conventional anticancer agents.²¹ Compound **5b** exhibited potent antiproliferative activity against the Caki-1 cells (Table 2). Because cell proliferation is generally regulated by controlling cell cycle progression, the cell cycle distribution of Caki-1 cells treated with **5b** for 24 h was analyzed by flow cytometry.²² Treatment with **5b** was demonstrated to induce G0/G1 cell cycle arrest in a concentration-dependent manner (Figure 2A). The G0/G1

cell cycle arrest by **5b** was also found to be stronger than that caused by the parent natural product **2**. When the expression of proteins associated with G0/G1 cell cycle progression was examined further, the expression of cyclin A2, cyclin D1, cyclin E, c-myc, and phosphorylated-Rb (p-Rb) was found to be suppressed by **5b** in a concentration-dependent manner (Figure 2B). Previous studies reported that the phenanthroindolizidine alkaloids antofine, tylophorine, and their analogues also induce cell cycle arrest at the G0/G1 phase.^{10e,12} Therefore, the induction of G0/G1 cell cycle arrest by **5b** seems to be a common feature of the antiproliferative activity of phenanthroindolizidine alkaloids against cancer cells.

Recent work by Yang et al. revealed that the accumulation of p-c-Jun, which is phosphorylated by c-Jun N-terminal protein kinase (JNK), is responsible for cell cycle arrest in G0/G1.^{10e} To further explore the association of JNK in the cell cycle arrest induced by **5b**, Western blot analysis was performed on Caki-1 cells after treatment with **5b** for 24 h. As shown in Figure 2C,

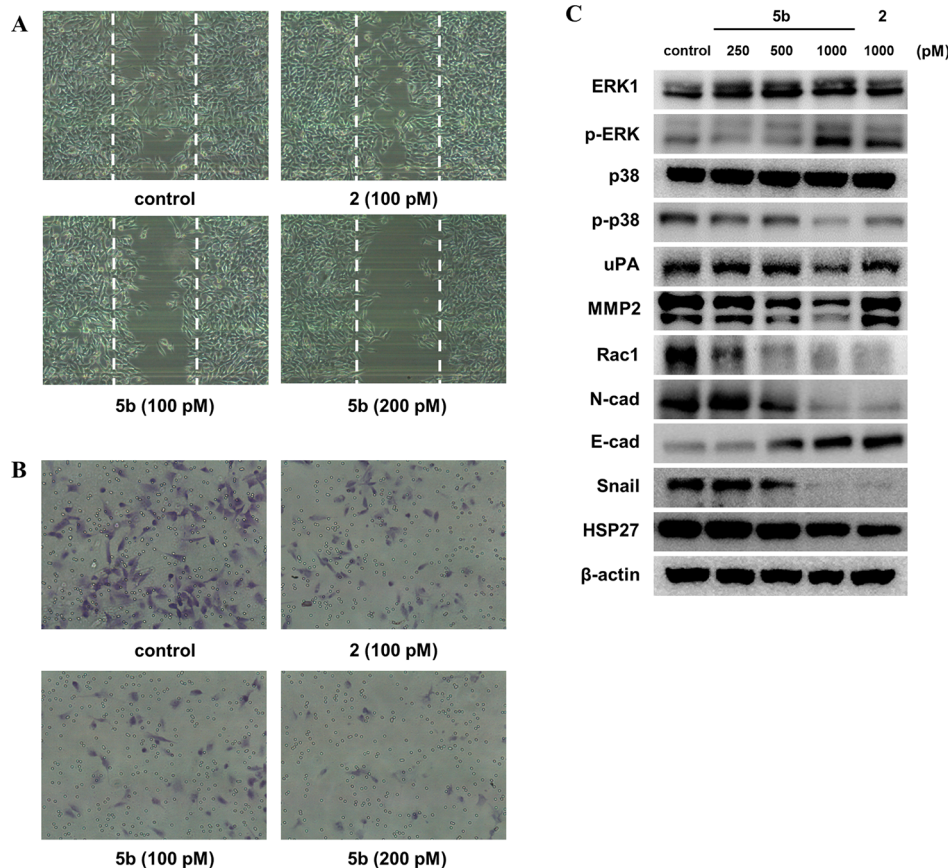


Figure 4. Effects of **5b** on cell migration and invasion. (A) Wound-healing assay in Caki-1 cells. Cells were seeded in six-well plates and incubated for 48 h. An artificial wound was made that consisted of a scratch with a micropipet tip. The wound-closing process was monitored over a 24 h incubation with the indicated concentrations of **5b**. Wounds were photographed at 24 h on an inverted microscope. (B) Invasion assay of Caki-1 cells. Cells were plated in the upper chambers of Matrigel-coated transwell insert. The lower chamber contained 0.1 mg/mL BSA as a chemoattractant in the medium. The inserts were incubated for 24 h. Subsequently, the cells that had invaded the outer surface of the membrane were fixed, stained, and photographed. The parent compound, **2**, was used as the reference compound. (C) Western blot analysis of Caki-1 cells. Cells were treated with the indicated concentrations of **5b** for 24 h.

the expression of JNK, p-JNK, c-Jun, and p-c-Jun was up-regulated by **5b** treatment. These findings suggest that the regulation of cell cycle progression by **5b** is in part correlated with the activation of the JNK pathway. Similar results were also reported following treatment with the phenanthroindolizidine alkaloid tylophorine in various cancer cells.^{10e}

Regulation of NNMT Expression. Nicotinamide N-methyltransferase (NNMT) catalyzes the N-methylation of nicotinamide, pyrimidine, and other structurally related compounds. NNMT also plays an important role in the biotransformation of many xenobiotics.²³ In addition, NNMT is markedly overexpressed in various types of cancer.²⁴ In particular, NNMT is considered a potential tumor marker of renal cell carcinoma.²⁵ When we analyzed the expression of NNMT, we observed high NNMT expression levels in Caki-1 cells. However, treatment with **5b** for 24 h down-regulated NNMT expression in a concentration-dependent manner (Figure 3A). Recent studies also reported that NNMT is involved in cancer cell proliferation and survival, as well as cell cycle regulation.²⁶ To examine whether the effects of **5b** on cell proliferation and cell cycle regulation are associated with the expression of NNMT, siRNA experiments were conducted. The selected stealth siRNA for NNMT effectively suppressed the NNMT expression at both the mRNA and protein level (Figure 3B). As shown in Figure 3C, however, the

antiproliferative activity of **5b** was significantly lower in NNMT siRNA-transfected cells compared with the non-transfected and scrambled siRNA-transfected cells at all tested concentrations. The **5b**-induced G0/G1 cell cycle arrest was also abrogated in the NNMT siRNA transfected cells (Figure 3D). Further studies were then performed to confirm the involvement of NNMT in the regulation of JNK activation by **5b**. We found that NNMT siRNA transfection blocked JNK activation by **5b** (Figure 3E). These results suggest that the antiproliferative and cell cycle regulating effects of **5b** are, at least in part, associated with NNMT-dependent JNK activation in Caki-1 cells.

Regulation of Cell Invasion and Migration via the p38 MAPK Pathway. To further explore the biological activity of **5b**, the antimetastatic potential of this compound was evaluated by assaying the inhibition of cancer migration and invasion. Cell migration was assessed based on wound healing activity. A scratch-wound in vehicle-treated control cells was clearly closed after 24 h incubation. However, treatment with **5b** effectively inhibited wound closure in a concentration-dependent manner (Figure 4A). In addition, the aggressive invasion potential of Caki-1 cells through a Matrigel-embedded chamber system was also effectively inhibited in a concentration-dependent manner upon treatment with **5b**, and over 90% inhibition was exhibited even at 200 pM **5b** (Figure 4B). These findings suggest that **5b**

Table 4. Pharmacokinetic Properties of **5b** and **2** in Mice^a

compd	intravenous dose, 1 mg/kg ^b				oral dose, 10 mg/kg ^b			
	CL ^c (L h ⁻¹ kg ⁻¹)	T _{1/2} ^d (h)	V _{ss} ^e (L/kg)	AUC ^f (ng·h/mL)	C _{max} ^f (ng/mL)	T _{1/2} ^g (h)	AUC ^e (ng·h/mL)	F ^h (%)
5b	12.5 ± 3.5	1.2 ± 0.1*	19.1 ± 5.5	84.0 ± 20.4	78.8 ± 9.9	1.8 ± 0.2	251.0 ± 43.9***	29.9 ± 4.5**
2	19.0 ± 2.2	0.9 ± 0.1	16.3 ± 2.0	53.2 ± 6.5	75.8 ± 77.6	nd ⁱ	52.7 ± 44.7	9.9 ± 8.4

^aPharmacokinetic parameters were estimated using a noncompartmental analysis of the mean plasma concentration versus time profile after oral and intravenous administration. Data are the mean ± SD ($n = 3\text{--}6$). (*) $p < 0.05$, (**) $p < 0.01$, (*** $p < 0.001$ by *t*-test versus **2**). ^bDosed as a solution prepared in a 1:9 (v/v) mixture of dimethylacetamide and 20 w/v aqueous 2-hydroxypropyl- β -cyclodextrin. ^cClearance. ^dVolume of distribution at steady state. ^eAUC (area under the curve) from hour zero to infinity except for the oral dose of **2**, where the value was from hour zero to the last quantifiable time point. ^fMaximum concentration observed. ^gHalf-life. ^hOral bioavailability. ⁱNot determined, as the terminal phase could not be clearly identified in the plasma concentration–time curves of individual animals.

exhibits antimetastatic potential against cancer cells. To further elucidate the mechanism of the inhibition of cancer cell migration and invasion, the expression of cellular signaling molecules was determined by Western blot analysis. Mitogen-activated protein kinases (MAPKs) play an important role in the regulation of cell growth, migration, and the control of cellular responses to cytokines and stress. Therefore, the expression levels of MAPKs in Caki-1 cells were examined after treatment with **5b** for 24 h. As shown in Figure 4C, the expression of ERK1 and p-ERK was elevated, while that of p-p38 was down-regulated. The functions of MAPKs in cancer cells are complex and poorly understood. Although the effects of p38 on cell proliferation are cell-type specific, p38 is thought to directly affect tumor invasion, migration, and metastasis. For example, the expression of matrix metalloproteinases (MMPs), urokinase-type plasminogen activator (uPA), Rac1, Snail, and E-cadherin is correlated with the activation of p38 MAPK.²⁷ p38 also affects the actin cytoskeleton by regulating the 27 kDa heat shock protein (HSP27).²⁸ Therefore, the expression levels of these proteins, which are regulated by p38, were examined in Caki-1 cells after treatment with **5b** for 24 h (Figure 4C). The expression of metastasis-associated proteins, uPA, MMP2, and Rac1, was suppressed by **5b**. In addition, when we analyzed the expression of epithelial-mesenchymal transition (EMT) related proteins, N-cadherin, an EMT activator, was down-regulated, whereas E-cadherin, an EMT inhibitor, was up-regulated. The expression of Snail, which can repress E-cadherin transcription, was also down-regulated. The expression of HSP27 was also down-regulated by **5b**, indicating the deregulation of the actin cytoskeleton by **5b** in Caki-1 cells. These results suggest that **5b** effectively suppressed the invasion and migration of Caki-1 renal cancer cells through the regulation of the p38 MAPK signaling pathway.

Solubility and Oral Bioavailability of **5b.** To investigate whether our structural modifications improved the druglikeness, the aqueous solubility and pharmacokinetic properties of **5b** were investigated and compared with those of the parent alkaloid **2**. The thermodynamic aqueous solubilities of cryptopleurine (**2**) and its sulfonamide analogue **5b** were determined according to Avdeef and Testa.²⁹ In our calculations (Table 1), compound **5b** was calculated to have higher solubility relative to the parent natural compound. In our actual solubility experiments, we found the results to be congruent with the calculations; sulfonamide analogue **5b** displayed better solubility (6.95 μ g/mL) than cryptopleurine **2** (<1 μ g/mL) in phosphate buffer (pH 7.4). In a 1:1 mixture of phosphate buffer and EtOH, the solubility of **5b** was 3 times higher than that of **2** (513 μ g/mL vs 160 μ g/mL).

Pharmacokinetic studies were carried out in male ICR mice using an intravenous dose of 1 mg/kg and an oral dose of 10

mg/kg. Compound **5b** had a lower systemic clearance (CL) than **2** following the intravenous dose (Table 4). Both compounds had a high volume of distribution (V_{ss}) that was well in excess of total body water (i.e., ~0.6 L/kg) (Table 4). The oral dose of **5b** exhibited a bioavailability (*F*) of 29.9%, which was approximately 3 times higher than that of **2** (Table 4). The half-life ($T_{1/2}$) of **5b** appeared to be longer than that of **2** following oral administration judging from the slopes of the apparent terminal phases in their mean plasma concentration–time curves (Figure 5), although the $T_{1/2}$ of **2** could not be determined due to lack of clearly identified terminal phase in its plasma concentration–time curves of individual mice (Table 4). Moreover, the coefficient of variation (CV) values of the

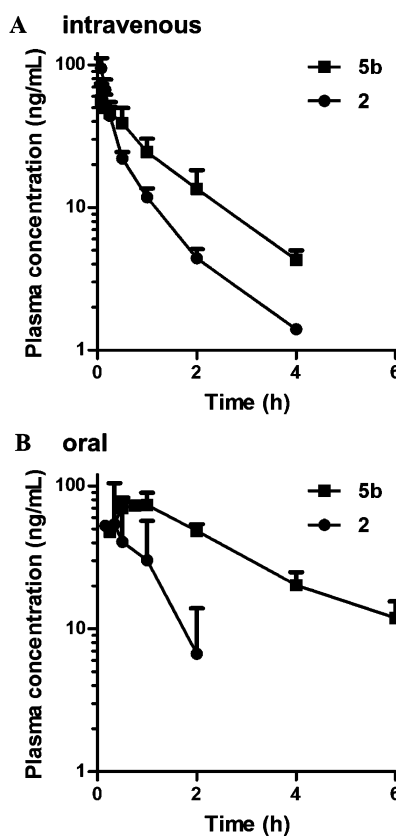


Figure 5. Plasma concentration–time curves of **2** and **5b** following a single intravenous or oral dose in mice. (A) Male ICR mice were given a single intravenous (1 mg/kg) dose of **2** or **5b**. (B) Male ICR mice were given a single oral (10 mg/kg) dose of **2** or **5b**. Plasma samples taken at selected times for 24 h after dosing were analyzed by LC–MS/MS for quantitation of the test compounds. Data are shown as the mean ± SD ($n = 3\text{--}6$).

oral pharmacokinetic parameters were drastically reduced, from 85–102% for **2** to 11–17% for **5b** (Table 4), suggesting that **5b** has much lower variability in oral absorption than **2**. Overall, **5b** exhibited a superior pharmacokinetic profile compared with **2** in mice, especially after oral administration. These results indicated that physicochemical and pharmacokinetic properties of natural product were improved in response to the introduction of polar sulfonamide group at C-6.

In Vivo Antitumor Activity. On the basis of the potent in vitro antiproliferative effect and the improved pharmacokinetic properties of **5b** compared with the parent compound (*R*)-cryptopleurine, the in vivo antitumor activity of **5b** was further determined using a nude-mouse xenograft model. Nude mice subcutaneously engrafted with Caki-1 cells were randomized to receive oral administration of either the vehicle (normal saline) or **5b** (1 or 3 mg/kg). At the termination of the experiment (42 days after inoculation), tumor volumes in the control group were approximately 890 mm³. Compared with the control group, tumor growth was significantly inhibited after **5b** treatment. The inhibition rates of the tumor size relative to the control volume were 64.6% and 76.0% at 1 mg/kg and 3 mg/kg of **5b**, respectively (Figure 5A). In addition, the body weight change and overt toxicity were negligible for **5b** administration (Figure 5B).³⁰ These data indicate that **5b** exhibits potential orally active antitumor activity without overt toxicity.

To further verify these findings in in vitro, biochemical analyses of tumor tissues were conducted. As shown in Figure 6C, the expression of proliferating cell nuclear antigen (PCNA), a proliferation biomarker, was markedly suppressed in the tumors of the **5b**-treated mice compared with the vehicle-treated control tumor tissues. The protein level of NNMT, an important tumor marker of renal cell carcinoma, was also down-regulated, but the expression of p-JNK was up-regulated in the **5b**-treated group. In addition, p-p38, a cell migration and invasion-associated marker, was down-regulated in the **5b**-treated mice. The ex vivo tissue analysis of tumor biomarkers was in good agreement with the findings from the in vitro cell culture systems. Overall, these data suggest that **5b** effectively inhibits the growth of Caki-1 cell tumor xenografts by regulating NNMT, p-JNK, and p-p38 expression.

CONCLUSION

Although phenanthroindolizidine and phenanthroquinolizidine alkaloids, represented here by antofine and cryptopleurine, have a profound antiproliferative activity and unique mode of action, they must be structurally modified to be clinical candidates because of their many pharmacologically unsuitable properties. With the hope of improving the druglikeness of these compounds by introducing polar groups, we have rationally designed, synthesized, and evaluated polar analogues in which the C-6 methoxy group of the natural alkaloids was replaced with a methanesulfonamide group. The methanesulfonamide analogue of antofine exhibited similar antiproliferative activity compared with the parent natural product, whereas the analogue of cryptopleurine, **5b**, was approximately 2- to 3-fold more active against various cancer cells. Compound **5b** exhibited improved pharmacokinetic properties, including a higher clearance, a longer half-life, and a higher oral bioavailability, compared with its parent natural product. Studies of mechanism of action suggest that the inhibition of cancer cell growth by **5b** is associated with the induction of G0/G1 cell cycle arrest via nicotinamide N-methyltransferase-

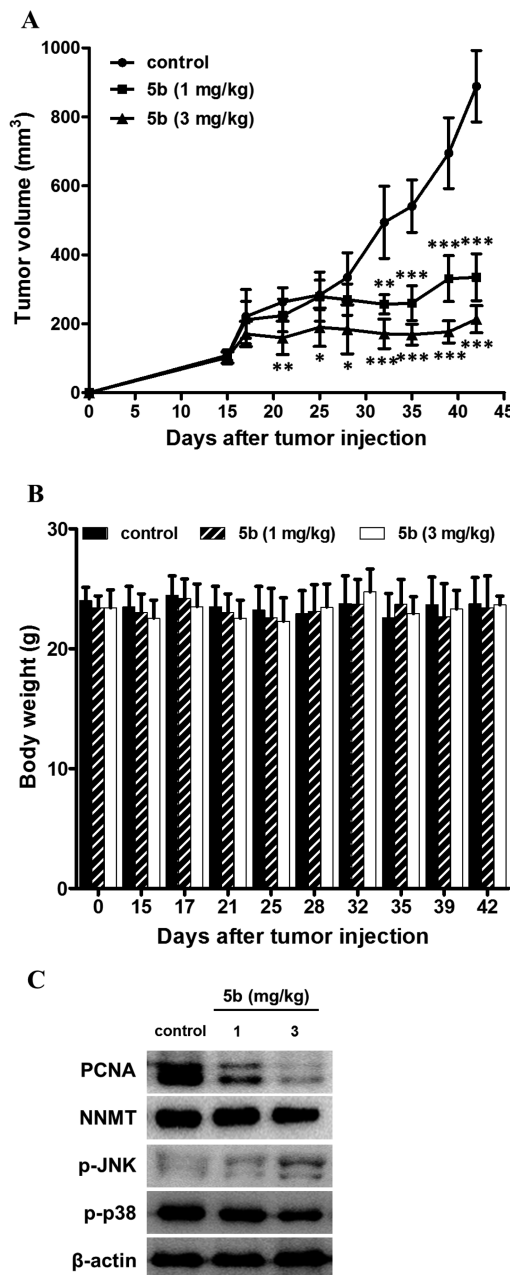


Figure 6. Antitumor activity of orally active **5b**. (A) The antitumor activity of **5b**. Caki-1 cells (1×10^7 cells/mouse) were subcutaneously injected into the flanks of nude mice. Treatment with the test compounds was initiated when tumor volumes reached ~ 100 mm³. **5b** (1 and 3 mg/kg body weight) was orally administered 5 times per week in a volume of 200 μ L. The control group was treated with an equal volume of vehicle. Compound **2** (3 mg/kg body weight) was used as the reference compound. Tumor volumes were measured with a caliper every 2–3 days. (B) Body weight change in the tumor xenograft model. Body weights were monitored every 2–3 days. (*) $p < 0.05$, (**) $p < 0.01$, (***) $p < 0.001$ by *t*-test. (C) Ex vivo biochemical analysis of tumors. Small portions of the tumors from each group were thawed on ice and homogenized in complete lysis buffer. The expression levels of the biomarker proteins were determined by Western blot analysis.

dependent JNK activation in Caki-1 renal cancer cells. In addition, compound **5b** significantly inhibited the migration and invasion of Caki-1 cancer cells by modulating the p38 MAPK signaling pathway. The improved bioavailability and

significant antitumor activity of methanesulfonamide analogue **5b** suggest that it is a promising new anticancer agent with a unique mode of action that is different from those of currently available anticancer drugs. Further studies of the pharmacological and metabolic features of **5b** will be reported in due course.

EXPERIMENTAL SECTION

General Methods for Chemistry. All chemicals were reagent grade and used as purchased. All reactions were performed under an inert atmosphere of dry nitrogen using distilled dry solvents. Reactions were monitored via TLC analysis using silica gel 60 F-254 thin-layer plates. Compounds were visualized on the TLC plates under UV light and by spraying with either KMnO₄ or anisaldehyde solutions. Flash column chromatography was conducted on silica gel 60 (230–400 mesh). Melting points were measured using a Buchi B-540 melting point apparatus without correction. ¹H NMR (400, 500, or 600 MHz) and ¹³C NMR (75, 100, 125, or 150 MHz) spectra were recorded in δ units using residual CHCl₃ (δ 7.24 ppm) and CDCl₃ (δ 77.0 ppm) as an internal standard. The IR spectra were measured on a Fourier transform infrared spectrometer. High-resolution mass spectra (HRMS) were recorded using FAB. All final target compounds were characterized and determined to be least >95% pure by analytical HPLC (Agilent 1200 series, Agilent Technologies, Palo Alto, CA, USA) using the following method. Mobile phase A consisted of 0.1% formic acid in HPLC-grade water. HPLC analysis was performed using a reverse-phase Agilent Eclipse Plus C18 column (4.6 mm \times 100 mm, 3.5 μ m) at a flow rate of 0.7 mL/min (30–100% aqueous MeOH with 0.1% formic acid over 20 min and MeOH with 0.1% formic acid from 20 to 25 min).

tert-Butyl (R)-2-(2-(3,4-Dimethoxyphenyl)-2-oxoethyl)-pyrrolidine-1-carboxylate (7a). To a stirred solution of magnesium (1.9 g, 78.2 mmol) in 80 mL of dry THF was added 4-bromoveratrole (8.5 mL, 59.1 mmol), and the mixture was heated at reflux for 2 h to generate the Grignard reagent. After cooling to room temperature, **6a** (4.11 g, 42.2 mmol) was added to the Grignard reagent, which was stirred for another 3 h at room temperature. The reaction was quenched with saturated aqueous NH₄Cl solution at 0 °C, diluted with H₂O, and extracted with EtOAc. The organic layer was dried with MgSO₄ and concentrated in vacuo. The crude product was separated through a short column using hexane/EtOAc as the eluent. The solvent was evaporated, and the residue was redissolved in 130 mL of CH₂Cl₂. 4 Å molecular sieves (9 g) and PCC (21.3 g, 99 mmol) were added at room temperature, and the reaction mixture was stirred for 2 h. The suspension was then filtered over a Celite pad, and the filtrate was concentrated in vacuo. The crude product was separated by silica gel column chromatography (hexane/EtOAc, 2:1) to give the desired ketone **7a** (18 g, 65%) as a pale yellow solid. Mp 92.5–94.0 °C; $[\alpha]_D^{20}$ 3.1 (c 0.77, CHCl₃); ¹H NMR (400 MHz, CDCl₃) δ 7.67 (brs, 1H), 7.58 (s, 1H), 6.88 (d, J = 8.4 Hz, 1H), 4.31–4.26 (m, 1H), 3.92 (s, 6H), 3.60 (brs, 1H), 3.35 (t, J = 5.7 Hz, 2H), 2.72 (brs, 1H), 2.02–1.97 (m, 1H), 1.91–1.74 (m, 3H), 1.44 (s, 9H); ¹³C NMR (75 MHz, CDCl₃) δ 197.6, 154.3, 153.2, 148.9, 130.0, 123.2, 110.1, 110.0, 79.4, 56.1, 56.0, 54.6, 46.4, 43.1, 30.6, 28.5 (3C), 23.2; IR (CHCl₃) ν_{max} 2973, 1688, 1396, 1271, 1169, 1024, 768 (cm⁻¹). HRMS (FAB): calcd for C₁₉H₂₈NO₅ [M + H]⁺ 350.1967, found 350.1965.

tert-Butyl (R)-2-(2-(3,4-Dimethoxyphenyl)-2-oxoethyl)-piperidine-1-carboxylate (7b). This compound was prepared from **6b** (3.21 g, 14.1 mmol) according to the procedure for the synthesis of **7a**. The crude product was separated by silica gel column chromatography (hexane/EtOAc, 2:1) to give the desired ketone **7b** (3.23 g, 63%) as a pale yellow solid. Mp 116.8–118.0 °C; $[\alpha]_D^{20}$ –41.4 (c 0.35, CHCl₃); ¹H NMR (400 MHz, CDCl₃) δ 7.60 (d, J = 7.8 Hz, 1H), 7.52 (s, 1H), 6.85 (d, J = 8.4 Hz, 1H), 4.78–4.72 (m, 1H), 3.98 (d, J = 11.8 Hz, 1H), 3.89 (s, 3H), 3.89 (s, 3H), 3.09 (d, J = 7.4 Hz, 2H), 2.84 (t, J = 12.7 Hz, 1H), 1.65–1.51 (m, 4H), 1.45–1.26 (m, 2H), 1.34 (s, 9H); ¹³C NMR (100 MHz, CDCl₃) δ 197.1, 154.7, 153.3, 149.0, 130.1, 123.0, 110.4, 110.0, 79.4, 56.0, 55.9, 48.5, 39.4, 38.8, 28.2 (3C), 28.0, 25.2, 18.8; IR (CHCl₃) ν_{max} 2936, 1687, 1415,

1268, 1160, 1024, 873, 768 (cm⁻¹). HRMS (FAB): calcd for C₁₉H₂₈NO₅ [M + H]⁺ 350.1967, found 350.1965.

(R)-1-(3,4-Dimethoxyphenyl)-2-(1-(2-(4-nitrophenyl)acetyl)-pyrrolidin-2-yl)ethan-1-one (8a). To a stirred solution of **7a** (2.62 g, 7.2 mmol) in 20 mL of CH₂Cl₂ was added TFA (5 mL) at room temperature, and the reaction mixture was stirred for 2 h. The reaction mixture was basified with 1 N NaOH and extracted with EtOAc. The solvent was concentrated in vacuo, and the crude amine was used for the next reaction without further purification. To a stirred solution of 4-nitrophenylacetic acid (1.57 g, 8.7 mmol) in 20 mL of CH₂Cl₂ were added EDCI (1.50 g, 7.9 mmol), DMAP (965 mg, 7.9 mmol), and the obtained amine (1.90 g, 7.2 mmol) at room temperature, and the reaction mixture was stirred for 15 h. The reaction was quenched with 1 N HCl at room temperature, diluted with H₂O, and extracted with CH₂Cl₂. The organic layer was dried over MgSO₄ and concentrated in vacuo. The crude product was separated by silica gel column chromatography (hexane/EtOAc, 1:3) to give an amide **8a** (2.60 g, 84%) as a white waxy solid. $[\alpha]_D^{20}$ –16.0 (c 0.21, CHCl₃); ¹H NMR (500 MHz, CDCl₃) δ 8.17 (d, J = 8.5 Hz, 2H), 7.78 (d, J = 8.4 Hz, 1H), 7.57 (s, 1H), 7.43 (d, J = 8.4 Hz, 2H), 6.87 (d, J = 8.5 Hz, 1H), 4.54–4.51 (m, 1H), 3.91 (s, 3H), 3.91 (s, 3H), 3.78 (dd, J = 2.5 Hz, 14.3 Hz, 1H), 3.71 (s, 2H), 3.58–3.54 (m, 1H), 3.49–3.44 (m, 1H), 2.64 (dd, J = 10.4 Hz, 14.0 Hz, 1H), 2.07–1.88 (m, 4H); ¹³C NMR (125 MHz, CDCl₃) δ 197.2, 168.1, 153.4, 149.0, 147.0, 142.3, 130.2 (2C), 129.7, 123.7 (2C), 123.6, 110.2, 110.1, 56.03, 56.0, 55.5, 47.5, 41.85, 41.75, 29.3, 23.9; IR (CHCl₃) ν_{max} 2969, 1639, 1516, 1413, 1345, 1269, 1151, 1022, 757 (cm⁻¹). HRMS (FAB): calcd for C₂₂H₂₅N₂O₆ [M + H]⁺ 413.1713, found 413.1704.

(R)-1-(3,4-Dimethoxyphenyl)-2-(1-(2-(4-nitrophenyl)acetyl)-piperidin-2-yl)ethan-1-one (8b). This compound was prepared from **7b** (2.21 g, 6.08 mmol) according to the procedure for the synthesis of **8a**. The crude product was separated by silica gel column chromatography (hexane/EtOAc, 1:3) to give the desired amide **8b** (2.05 g, 79%) as a white waxy solid. $[\alpha]_D^{20}$ 8.7 (c 0.91, CHCl₃); ¹H NMR (600 MHz, CDCl₃, amide rotamers) δ 8.11 (d, J = 8.7 Hz, 0.8H), 8.08 (d, J = 8.7 Hz, 1.2H), 7.68 (dd, J = 1.8 Hz, 8.3 Hz, 0.4H), 7.50 (d, J = 1.8 Hz, 0.4H), 7.47 (dd, J = 1.8 Hz, 8.3 Hz, 0.6H), 7.43 (d, J = 2.3 Hz, 0.6H), 7.42 (d, J = 8.7 Hz, 1.2H), 7.34 (d, J = 8.8 Hz, 0.8H), 6.85 (t, J = 8.7 Hz, 1H), 5.23 (td, J = 4.8 Hz, 8.7 Hz, 0.4H), 4.72 (q, J = 5.6 Hz, 0.6H), 4.55 (d, J = 13.3 Hz, 0.6H), 3.95 (q, J = 15.2 Hz, 1.2H), 3.91 (s, 1.8H), 3.90 (s, 1.8H), 3.88 (s, 2.4H), 3.76 (td, J = 11.2 Hz, 12.7 Hz, 0.8H), 3.65 (d, J = 11.5 Hz, 0.4H), 3.17 (d, J = 6.6 Hz, 2H), 3.14–3.04 (m, 0.6H), 2.62 (td, J = 2.6 Hz, 13.4 Hz, 0.4H), 1.67–1.52 (m, 4H), 1.45–1.26 (m, 2H); ¹³C NMR (150 MHz, CDCl₃) δ 196.6, 195.8, 168.41, 168.38, 153.8, 153.4, 149.2, 149.0, 146.8, 146.7, 143.3, 142.8, 129.9, 129.8, 129.7, 129.6, 123.60, 123.55, 123.2, 122.6, 110.2, 110.1, 110.0, 109.9, 56.0, 55.94, 55.88, 49.5, 46.8, 42.0, 40.7, 40.5, 38.6, 38.4, 37.5, 29.5, 27.2, 25.5, 25.2, 19.2, 18.5; IR (CHCl₃) ν_{max} 2936, 1638, 1517, 1418, 1345, 1265, 1153, 1021, 753 (cm⁻¹). HRMS (FAB): calcd for C₂₃H₂₇N₂O₆ [M + H]⁺ 427.1869, found 427.1877.

(R)-7-(3,4-Dimethoxyphenyl)-6-(4-nitrophenyl)-2,3,8,8a-tetrahydroindolin-5(1H)-one (9a). To a stirred solution of amide **8a** (2.20 g, 6.05 mmol) in 30 mL of EtOH was added K₂CO₃ (300 mg) at room temperature, and the reaction mixture was refluxed for 1.5 h. The reaction mixture was cooled to room temperature and concentrated in vacuo. The reaction mixture was diluted with H₂O and extracted with CH₂Cl₂. The organic layer was dried over MgSO₄ and concentrated in vacuo. The crude product was separated by silica gel column chromatography (hexane/EtOAc, 1:1) to give an unsaturated amide **9a** (1.80 g, 85%) as a yellow solid. Mp 182.9–184.1 °C; $[\alpha]_D^{20}$ 3.5 (c 0.35, CHCl₃); ¹H NMR (500 MHz, CDCl₃) δ 8.02 (d, J = 8.7 Hz, 2H), 7.30 (d, J = 8.8 Hz, 2H), 6.67 (d, J = 8.4 Hz, 1H), 6.62 (dd, J = 1.8 Hz, 8.3 Hz, 1H), 6.38 (d, J = 1.8 Hz, 1H), 3.99–3.91 (m, 1H), 3.80 (s, 3H), 3.68 (t, J = 10.5 Hz, 1H), 3.61–3.55 (m, 1H), 3.51 (s, 3H), 2.90 (dd, J = 4.4 Hz, 16.6 Hz, 1H), 2.74 (dd, J = 14.0 Hz, 16.5 Hz, 1H), 2.31 (td, J = 5.8 Hz, 11.7 Hz, 1H), 2.12–2.07 (m, 1H), 1.93–1.83 (m, 1H), 1.76–1.68 (m, 1H); ¹³C NMR (125 MHz, CDCl₃) δ 162.9, 149.1, 148.3, 147.4, 146.4, 144.1, 132.2 (2C), 131.3, 130.6, 122.7 (2C), 121.3, 112.1, 110.7, 55.8, 55.6 (2C), 44.8, 37.5,

33.7, 23.1; IR (CHCl_3) ν_{max} 2963, 1641, 1597, 1516, 1342, 1258, 1139, 1025, 854, 747 (cm^{-1}). HRMS (FAB): calcd for $\text{C}_{22}\text{H}_{23}\text{N}_2\text{O}_5$ [M + H]⁺ 395.1607, found 395.1599.

(R)-2-(3,4-Dimethoxyphenyl)-3-(4-nitrophenyl)-1,6,7,8,9,9a-hexahydro-4H-quinolin-4-one (9b). This compound was prepared from 8b (740 mg, 1.74 mmol) according to the procedure for the synthesis of 9a. The crude product was separated by silica gel column chromatography (hexane/EtOAc, 1:1) to give the desired amide 9b (611 mg, 86%) as a yellow solid. Mp 133.8–134.6 °C; $[\alpha]_D^{20}$ −12.1 (c 0.66, CHCl_3); ¹H NMR (400 MHz, CDCl_3) δ 8.02 (d, J = 8.6 Hz, 2H), 7.24 (d, J = 8.8 Hz, 2H), 6.67 (d, J = 8.4 Hz, 1H), 6.62 (dd, J = 1.8 Hz, 8.4 Hz, 1H), 6.35 (d, J = 1.5 Hz, 1H), 4.51 (d, J = 13.5 Hz, 1H), 3.80 (s, 3H), 3.64–3.58 (m, 1H), 3.50 (s, 3H), 2.89 (dd, J = 5.6 Hz, 17.5 Hz, 1H), 2.74 (dd, J = 10.7 Hz, 17.6 Hz, 1H), 2.64 (t, J = 13.0 Hz, 1H), 1.92–1.84 (m, 2H), 1.84–1.76 (m, 1H), 1.60–1.39 (m, 3H); ¹³C NMR (75 MHz, CDCl_3) δ 165.4, 149.0, 148.1, 147.3, 146.2, 144.4, 132.2 (2C), 131.0, 129.0, 122.6 (2C), 121.1, 111.8, 110.5, 55.7, 55.5, 53.7, 43.2, 37.3, 33.3, 24.6, 23.4; IR (CHCl_3) ν_{max} 2937, 1640, 1514, 1342, 1253, 1025, 853, 753 (cm^{-1}). HRMS (FAB): calcd for $\text{C}_{23}\text{H}_{25}\text{N}_2\text{O}_5$ [M + H]⁺ 409.1763, found 409.1754.

(R)-2,3-Dimethoxy-6-nitro-12,13,13a,14-tetrahydropyridobenzo-[f,h]pyrrolo[1,2-b]isoquinolin-9(11H)-one (10a). To a stirred solution of 9a (740 mg, 1.8 mmol) in 9 mL of CH_2Cl_2 was added phenyliodine(III) bis(trifluoroacetate) (PIFA) (860 mg, 2.0 mmol) and $\text{BF}_3\text{-OEt}_2$ (330 μL , 2.7 mmol) at −10 °C, and the reaction mixture was stirred for 15 min. The reaction mixture was quenched with sat. NaHCO_3 solution, diluted with H_2O , and extracted with CH_2Cl_2 . The organic layer was dried over MgSO_4 and concentrated in vacuo. The crude product was separated by silica gel column chromatography (CH_2Cl_2 /EtOAc, 10:1) to give an amide 10a (384 mg, 91%) as a yellow solid. Mp 289.1–291.0 °C; $[\alpha]_D^{20}$ −130.2 (c 0.23, CHCl_3); ¹H NMR (500 MHz, CDCl_3) δ 9.47 (d, J = 9.4 Hz, 1H), 9.30 (s, 1H), 8.27 (dd, J = 1.6 Hz, 9.2 Hz, 1H), 7.95 (s, 1H), 7.34 (s, 1H), 4.18 (s, 3H), 4.06 (s, 3H), 3.97–3.87 (m, 1H), 3.87–3.75 (m, 2H), 3.61 (dd, J = 3.6 Hz, 15.9 Hz, 1H), 2.93 (t, J = 14.5 Hz, 1H), 2.49–2.42 (m, 1H), 2.22–2.15 (m, 1H), 2.02–1.86 (m, 2H); ¹³C NMR (125 MHz, CDCl_3) δ 163.4, 151.4, 150.4, 145.1, 139.0, 132.5, 129.5, 128.9, 127.2, 124.5, 123.2, 119.5, 118.0, 104.9, 103.7, 56.3, 56.0, 55.0, 45.4, 33.8, 33.0, 23.5; IR (CHCl_3) ν_{max} 2969, 1637, 1516, 1440, 1338, 1264, 1207, 1030, 843, 749 (cm^{-1}). HRMS (FAB): calcd for $\text{C}_{22}\text{H}_{21}\text{N}_2\text{O}_5$ [M + H]⁺ 393.1450, found 393.1451.

(R)-2,3-Dimethoxy-6-nitro-11,12,13,14,14a,15-hexahydro-9H-dibenzo[f,h]pyrido[1,2-b]isoquinolin-9-one (10b). This compound was prepared from 9b (430 mg, 1.05 mmol) according to the procedure for the synthesis of 10a. The crude product was separated by silica gel column chromatography (CH_2Cl_2 /EtOAc, 10:1) to give 10b (384 mg, 90%) as a yellow solid. Mp 251.5–253.1 °C; $[\alpha]_D^{20}$ −190.2 (c 0.31, CHCl_3); ¹H NMR (400 MHz, CDCl_3) δ 9.70 (d, J = 9.5 Hz, 1H), 9.17 (d, J = 2.2 Hz, 1H), 8.20 (dd, J = 2.3 Hz, 9.5 Hz, 1H), 7.82 (s, 1H), 7.23 (s, 1H), 4.68 (d, J = 13.5 Hz, 1H), 4.14 (s, 3H), 4.04 (s, 3H), 3.58–3.51 (m, 1H), 3.37 (dd, J = 4.6 Hz, 16.7 Hz, 1H), 2.95 (dd, J = 11.2 Hz, 16.7 Hz, 1H), 2.88 (t, J = 12.5 Hz, 1H), 2.03 (d, J = 10.6 Hz, 1H), 1.91 (d, J = 11.8 Hz, 2H), 1.64–1.46 (m, 3H); ¹³C NMR (75 MHz, CDCl_3) δ 166.1, 151.4, 150.2, 144.7, 139.0, 132.8, 129.8, 128.9, 127.0, 123.9, 120.6, 119.3, 117.7, 104.5, 103.3, 56.3, 56.0, 52.1, 42.5, 33.2, 32.9, 24.5, 22.7; IR (CHCl_3) ν_{max} 2938, 1636, 1517, 1416, 1338, 1255, 1207, 1032, 840, 749 (cm^{-1}). HRMS (FAB): calcd for $\text{C}_{23}\text{H}_{23}\text{N}_2\text{O}_5$ [M + H]⁺ 407.1607, found 407.1600.

(R)-N-(2,3-Dimethoxy-9-oxo-9,11,12,13,13a,14-hexahydro-dibenzo[f,h]pyrido[1,2-b]isoquinolin-6-yl)methanesulfonamide (12a). A stirred solution of 9a (337 mg, 0.86 mmol) in 20 mL of MeOH was hydrogenated for 4 h at room temperature under balloon pressure in the presence of 10 wt % Pd/C (85 mg). The reaction mixture was filtered over a Celite pad, and the filtrate was concentrated in vacuo to afford crude aniline as a yellow solid. To a stirred solution of crude aniline in 10 mL of CH_2Cl_2 were added pyridine (88 μL , 1.0 mmol) and MsCl (80 μL , 1.0 mmol) at 0 °C, and the reaction mixture was stirred for 2 h at room temperature. The reaction mixture was quenched with sat. NaHCO_3 solution, diluted with H_2O , and extracted with CH_2Cl_2 . The organic layer was dried

over MgSO_4 and concentrated in vacuo. The crude product was separated by silica gel column chromatography (CH_2Cl_2 /MeOH, 40:1) to give an amide 12a (220 mg, 58%) as a pale yellow solid. Mp 296.5–297.4 °C; $[\alpha]_D^{20}$ −132.0 (c 0.11, CHCl_3); ¹H NMR (600 MHz, CDCl_3) δ 9.26 (d, J = 9.2 Hz, 1H), 8.37 (d, J = 1.8 Hz, 1H), 7.85 (s, 1H), 7.34 (dd, J = 2.1 Hz, 8.9 Hz, 1H), 7.31 (s, 1H), 7.06 (brs, 1H), 4.07 (s, 3H), 4.04 (s, 3H), 3.95–3.89 (m, 1H), 3.89–3.84 (m, 1H), 3.82–3.77 (m, 1H), 3.56 (dd, J = 4.1 Hz, 15.6 Hz, 1H), 2.99 (s, 3H), 2.91 (dd, J = 13.5 Hz, 15.3 Hz, 1H), 2.45–2.41 (m, 1H), 2.18–2.15 (m, 1H), 2.00–1.87 (m, 2H); ¹³C NMR (150 MHz, CDCl_3) δ 164.1, 150.6, 149.9, 134.8, 134.5, 130.4, 129.6, 126.5, 126.3, 124.3, 123.2, 119.9, 113.2, 104.8, 103.8, 56.04, 55.96, 55.2, 45.4, 39.3, 33.8, 32.7, 23.6; IR (CHCl_3) ν_{max} 3015, 2942, 1601, 1512, 1465, 1317, 1258, 1203, 1149, 1031, 980, 841, 747 (cm^{-1}). HRMS (FAB): calcd for $\text{C}_{23}\text{H}_{25}\text{N}_2\text{O}_5\text{S}$ [M + H]⁺ 441.1484, found 441.1479.

(R)-N-(2,3-Dimethoxy-9-oxo-11,12,13,14,14a,15-hexahydro-9H-dibenzo[f,h]pyrido[1,2-b]isoquinolin-6-yl)methanesulfonamide (12b). This compound was prepared from 10b (100 mg, 0.246 mmol) according to the procedure for the synthesis of 12a. The crude product was separated by silica gel column chromatography (CH_2Cl_2 /MeOH, 30:1) to give the desired amide 12b (62.6 mg, 56%) as a white solid. Mp 258.8–260.2 °C; $[\alpha]_D^{20}$ −183.2 (c 0.68, CHCl_3); ¹H NMR (500 MHz, CDCl_3) δ 9.49 (d, J = 9.2 Hz, 1H), 8.31 (s, 1H), 7.74 (s, 1H), 7.44 (brs, 1H), 7.35 (dd, J = 1.8 Hz, 9.2 Hz, 1H), 7.16 (s, 1H), 4.69 (d, J = 13.4 Hz, 1H), 4.00 (s, 6H), 3.55–3.51 (m, 1H), 3.30 (dd, J = 4.4 Hz, 16.4 Hz, 1H), 3.00 (s, 3H), 2.91–2.85 (m, 2H), 2.02–1.98 (m, 1H), 1.89 (d, J = 11.5 Hz, 2H), 1.66–1.43 (m, 3H); ¹³C NMR (100 MHz, CDCl_3) δ 166.9, 150.8, 149.9, 134.8, 134.3, 130.6, 130.2, 126.8, 126.7, 124.0, 120.9, 119.8, 113.3, 104.6, 103.8, 56.1, 56.0, 52.6, 42.6, 39.3, 33.0, 32.9, 24.6, 22.9; IR (CHCl_3) ν_{max} 3259, 2936, 1734, 1615, 1513, 1469, 1418, 1256, 1153, 1036, 969, 844, 753 (cm^{-1}). HRMS (FAB): calcd for $\text{C}_{24}\text{H}_{27}\text{N}_2\text{O}_5\text{S}$ [M + H]⁺ 455.1641, found 455.1634.

(R)-N-(2,3-Dimethoxy-9,11,12,13,13a,14-hexahydrodibenzo-[f,h]pyrrolo[1,2-b]isoquinolin-6-yl)methanesulfonamide (5a). To a stirred solution of 12a (140 mg, 0.32 mmol) in 6 mL of THF was added LiAlH_4 (0.48 mL, 0.48 mmol, 1 M solution in THF) at 0 °C, and the reaction mixture was refluxed for 2 h. The reaction mixture was quenched by successive addition of H_2O , a 15% NaOH aq solution, and H_2O . The suspension was then filtered over a Celite Pad, and the filtrate was concentrated in vacuo. The crude product was separated by silica gel column chromatography (CH_2Cl_2 /MeOH, 15:1) to give the desired product 5a (90 mg, 66%) as a white solid. Mp 244.5–245.2 °C; $[\alpha]_D^{20}$ −80.2 (c 0.21, CHCl_3); ¹H NMR (400 MHz, CDCl_3) δ 8.02 (s, 1H), 7.66 (d, J = 8.8 Hz, 1H), 7.58 (s, 1H), 7.29 (s, 1H), 7.29–7.27 (m, 1H), 4.56 (d, J = 14.9 Hz, 1H), 4.05 (s, 3H), 4.00 (s, 3H), 3.60 (d, J = 14.9 Hz, 1H), 3.49 (t, J = 8.1 Hz, 1H), 3.35 (dd, J = 2.5 Hz, 15.9 Hz, 1H), 3.00–2.94 (m, 1H), 2.98 (s, 3H), 2.57–2.40 (m, 2H), 2.30–2.20 (m, 1H), 2.18–2.00 (m, 1H), 2.00–1.89 (m, 1H), 1.89–1.78 (m, 1H); ¹³C NMR (100 MHz, CDCl_3) δ 149.6, 148.6, 133.6, 129.5, 128.0, 127.0, 126.7, 126.0, 124.0, 123.5, 120.5, 116.0, 103.8, 103.5, 60.3, 55.9, 55.8, 54.9, 53.6, 39.5, 33.7, 31.2, 21.6; IR (CHCl_3) ν_{max} 3015, 2942, 2831, 1601, 1512, 1317, 1258, 1203, 1149, 1031, 980, 841, 747 (cm^{-1}). HRMS (FAB): calcd for $\text{C}_{23}\text{H}_{27}\text{N}_2\text{O}_4\text{S}$ [M + H]⁺ 427.1692, found 427.1696.

(R)-N-(2,3-Dimethoxy-9-oxo-11,12,13,14,14a,15-hexahydro-9H-dibenzo[f,h]pyrido[1,2-b]isoquinolin-6-yl)methanesulfonamide (5b). This compound was prepared from 12b (100 mg, 0.22 mmol) according to the procedure for the synthesis of 5a. The crude product was separated by silica gel column chromatography (CH_2Cl_2 /MeOH, 15:1) to give the desired product 5b (60 mg, 62%) as a pale yellow solid. Mp 240.8–242.9 °C; $[\alpha]_D^{20}$ −69.6 (c 0.14, CHCl_3); ¹H NMR (400 MHz, CDCl_3) δ 8.05 (s, 1H), 7.67 (d, J = 8.8 Hz, 1H), 7.62 (s, 1H), 7.27 (dd, J = 1.5 Hz, 9.4 Hz, 1H), 7.24 (s, 1H), 4.32 (d, J = 15.4 Hz, 1H), 4.06 (s, 3H), 4.01 (s, 3H), 3.56 (d, J = 15.5 Hz, 1H), 3.29 (d, J = 11.3 Hz, 1H), 3.11 (d, J = 3.1 Hz, 16.5 Hz, 1H), 3.02–2.92 (m, 1H), 2.99 (s, 3H), 2.46–2.37 (m, 1H), 2.37–2.26 (m, 1H), 2.04 (d, J = 10.9 Hz, 1H), 1.90 (d, J = 12.2 Hz, 1H), 1.87–1.78 (m, 2H), 1.69–1.56 (m, 1H), 1.50–1.38 (m, 1H); ¹³C NMR (100 MHz, CDCl_3) δ 149.5, 148.5, 133.3, 129.3, 126.9, 126.4, 125.9, 124.7,

123.6, 123.4, 121.1, 117.4, 103.52, 103.48, 57.9, 56.3, 56.0, 55.9, 55.7, 39.6, 34.6, 33.3, 25.7, 24.3; IR (CHCl_3) ν_{max} 3013, 2934, 1609, 1512, 1323, 1257, 1203, 1152, 1034, 977, 845, 750 (cm^{-1}). HRMS (FAB): calcd for $\text{C}_{24}\text{H}_{29}\text{N}_2\text{O}_4\text{S}$ [$\text{M} + \text{H}]^+$ 441.1848, found 441.1858.

Cell Culture. Human lung cancer (A549), colon cancer (HCT-116), stomach cancer (SNU-638), breast cancer (MDA-MB-231), liver cancer (SK-Hep-1), prostate cancer (PC-3), and renal cancer (Caki-1) cell lines were obtained from the Korean Cell Line Bank. Cells were grown in medium (DMEM for MDA-MB-231, SK-Hep-1, and Caki-1 cells; RPMI 1640 medium for A549, HCT-116, SNU-638 and PC-3 cells) supplemented with 10% fetal bovine serum (FBS) and antibiotics—antimycotics (PSF: 100 units/mL penicillin G sodium, 100 $\mu\text{g}/\text{mL}$ streptomycin, and 250 ng/mL amphotericin B). All cells were incubated at 37 °C in a humidified atmosphere containing 5% CO_2 and were subcultured twice a week. Cells passaged more than 3 times were used for experiments.

Growth Inhibition Assay. The growth-inhibitory potential of the test compounds against various human cancer cells was determined via the sulforhodamine B (SRB) assay. Cells were seeded in 96-well plates at a density of 5×10^3 cells/well and treated with various concentrations of the test compounds for 72 h. Cells were fixed with 10% trichloroacetic acid solution for 30 min at 4 °C, washed 5 times with tap water, and dried in air. Cells were stained with 0.4% SRB in 1% acetic acid solution for 30 min at room temperature. After stained cells were washed to remove unbound dye, dried, and suspended in 10 mM Tris (pH 10.0), absorbance was measured at 515 nm. Cell viability was calculated by comparison with the absorbance of the vehicle-treated control group. IC_{50} values, i.e., the concentration at which 50% cell survival was observed, were determined by nonlinear regression analysis using TableCurve software.

Cell Cycle Analysis. Cell cycle dynamics were measured by flow cytometry. Caki-1 cells (4×10^5 cells/dish in 60 mm dishes) were incubated with test samples for 24 h. All adherent and floating cells were collected and washed twice with PBS. Cells were fixed with 70% ethanol overnight at -20 °C. Fixed cells were washed with PBS and then stained with 50 $\mu\text{g}/\text{mL}$ propidium iodide solution containing 50 $\mu\text{g}/\text{mL}$ RNase A for 30 min at room temperature. Fluorescence intensity was analyzed on a FACSCalibur flow cytometer (BD Biosciences, San Jose, CA, USA). A total of 30 000 cells were counted for each analysis, and the distributions of cells in each phase of the cell cycle was displayed as histograms.

Western Blot Analysis. Total cell lysates were prepared in RIPA buffer (50 mM Tris-HCl, pH 8.0, 150 mM NaCl, 1% NP-40, 0.5% sodium deoxycholate, 0.1% SDS). Protein concentrations were determined, and equal amounts of proteins were transferred to polyvinylidene fluoride membranes (Millipore, Bedford, MA, USA) and probed with the indicated antibodies. The blots were detected using an enhanced chemiluminescence detection kit (GE Healthcare, Little Chalfont, U.K.).

RNA Extraction and Real-Time PCR. Total cellular RNA was extracted using the TRI reagent (Invitrogen, Carlsbad, CA) and reverse-transcribed using the reverse transcription system (Promega, Madison, WI), according to the manufacturer's instructions. Real-time PCR was performed using iQ SYBR Green Supermix (Bio-Rad, Richmond, CA) according to the manufacturer's instructions. The thermocycling conditions utilized were 20 s at 95 °C; 40 cycles of 20 s at 95 °C, 20 s at 56 °C, and 30 s at 72 °C; 1 min at 95 °C; and 1 min at 55 °C. All experiments were performed in quadruplicate. Specific primers were designed using Roche Applied System (Basel, Swiss) and custom synthesized by Pioneer Corporation (Daejeon, Korea). The following sequences were used: NNMT F5'-TCCTTTAGGAGATCGTCGTAC-3'; R5'-GCTTGACCGCCTG-TCTAAC-3'; ATCB F5'-AGCACAAATGAAGATCAAGAT-3'; R5'-TGTAAACGCAACTAAGTCATA-3'.

The threshold cycle (C_T), indicating the fractional cycle number at which the amount of amplified target gene in each well reaches a fixed threshold, was determined using MJ Research Opticon Monitor software. Relative quantification, representing the difference in gene expression as measured by real-time quantitative PCR between the **5b**-treated group and the untreated control group, was calculated using

the comparative C_T method. The data were analyzed using the equation $2^{-\Delta\Delta C_T}$, where $\Delta\Delta C_T = [C_T \text{ of target gene} - C_T \text{ of housekeeping gene}]_{\text{treated group}} - [C_T \text{ of target gene} - C_T \text{ of housekeeping gene}]_{\text{untreated control group}}$. For the treated samples, $2^{-\Delta\Delta C_T}$ represents the fold-change in gene expression, normalized to the housekeeping gene β -actin, relative to the untreated control.

RNA Interference. RNA interference of NNMT was performed using a set of three stealth siRNAs (HSS107222, HSS107223, HSS10724) purchased from Invitrogen (Carlsbad, CA). The RNA interference efficiency of the three siRNAs was tested, and HSS107222 was ultimately selected. For transfection, reverse transfection was performed using Lipofectamine RNAiMAX (Invitrogen) according to the manufacturer's recommendations. Compounds were administered after 24 h of transfection, and the treated cells were incubated for 24 h.

Wound-Healing Assay. Caki-1 cells were seeded in six-well plates at a density of 1×10^5 cells/mL and incubated for 48 h until they reached 80–90% confluence. A confluent monolayer of Caki-1 cells was artificially wounded with a micropipet tip, and the detached cells were washed with serum-free medium, followed by treatment with **5b** in growth medium for 24 h. The cells were washed twice with PBS. The wounds were photographed at 0 and 24 h on an inverted microscope (CKX41, Olympus).

Cell Invasion Assay. Caki-1 cells (1×10^5 cells/chamber) were seeded into the top chambers of 24-well Matrigel-coated polyethylene terephthalate membrane inserts with 8 μm pores (Millipore, Billerica, MA). The plates were coated with 10 μL of type I collagen (0.5 mg/mL) and 20 μL of a 1:2 mixture of Matrigel/RPMI 1640. Cells were plated in the upper chamber of the Matrigel-coated Transwell insert. The medium of the lower chambers also contained 0.1 mg/mL bovine serum albumin as a chemoattractant. The inserts were incubated for 24 h at 37 °C. The cells that had invaded the outer surface of the membrane were fixed with methanol, stained with hematoxylin and eosin, and photographed.

Pharmacokinetic Studies in Mice. All animal use and care followed the guidelines approved by the Institutional Animal Care and Use Committee of Korea University (Approval No. KUIACUC-2012-176). Male ICR mice (8 weeks old) were purchased from Koatech Co. (Pyeontak, Kyonggi-do, Republic of Korea). Animals were acclimatized for 1 week at of 23–25 °C temperature, 40–70% relative humidity, and 12 h light/12 h dark cycle before study. Dosing solutions were prepared in a 1:9 (v/v) mixture of dimethylacetamide and 20 w/v aqueous 2-hydroxypropyl- β -cyclodextrin at a concentration of 0.2 and 1 mg/mL for intravenous and oral dosing, respectively. Two groups of animals ($n = 3/\text{group}$) received either **5b** or **2** intravenously via tail-vein injection at a dose of 1 mg/kg. Another two groups of mice were orally administered either **5b** ($n = 3$) or **2** ($n = 6$) at a dose of 10 mg/kg. An amount of approximately 80 μL of blood samples was collected into BD Microtainer plasma separator tubes at selected times through the saphenous vein over 24 h after dosing. Blood samples were centrifuged at 6000g for 5 min and stored in a freezer until analysis. Protein precipitation was conducted on 15 μL of plasma samples using 3 volumes of acetonitrile containing carbamazepine as an internal analytical standard. After centrifugation, the supernatant was analyzed on an Agilent 6460 LC-ESI/MS/MS system coupled with an Agilent 1290 Infinity HPLC system. Chromatographic separation was performed on a Phenomenex Kinetex C18 column (2.0 mm × 50 mm, 2.6 μm) running a linear gradient of solvent A (0.1% formic acid in deionized water) and B (0.1% formic acid in acetonitrile). Detection of the analyte ions was performed in a positive MRM mode, monitoring the following precursor → product ion transitions: m/z 378 → 84, 441 → 84, and 237 → 194 for **2**, **5b**, and carbamazepine, respectively. Analytical data were processed using MassHunter B04.01 (Agilent Korea, Seoul, Republic of Korea). Pharmacokinetic parameters were calculated via noncompartmental analysis of the plasma concentration–time profiles using PK Solver.

In Vivo Tumor Xenograft Model. All animal use and care followed the guidelines approved by the Seoul National University Institutional Animal Care and Use Committee (IACUC; permission number SNU-121114-1-1). Female nude mice (4–6 weeks old,

BALB/c-nu) were purchased from Central Laboratory Animal, Inc. (Seoul, Korea) and housed in the animal care facility at Seoul National University under pathogen-free conditions with a 12 h light–dark schedule. After animals were acclimated for 1 week, Caki-1 cells were subcutaneously injected into the flanks of mice (1×10^7 cells in 200 μL medium) using 26.5 gauge needles. The resulting tumors were allowed to develop for 8 days until they reached approximately 100 mm³. The mice were randomized into vehicle control and treatment groups of five animals per group. **5b** (1 and 3 mg/kg body weight) was dissolved in 200 μL of vehicle solution (0.5% Tween 80 in normal saline) and orally administered 5 times a week for 4 weeks. The control group was treated with an equal volume of vehicle. Tumor growth was measured using a digital slide caliper, and tumor volume was estimated according to the following formula: tumor volume (mm³) = $L \times W \times H/2$, where L is the length, W is the width, and H is the height of the tumor. The experiment was terminated when the average tumor volume of the control group reached approximately 890 mm³. The mice were euthanized, and the tumors were excised, weighed, and frozen for further biochemical analysis. Toxicity was assessed based on the lethality and body weight loss exhibited by the nude mice.

Ex Vivo Biochemical Analysis of Tumors. A portion of the frozen tumor excised from each of the nude mice was thawed on ice and homogenized using a hand-held homogenizer in Complete lysis buffer (Active Motif, Carlsbad, CA). The protein concentrations of the tumor lysates were determined, and aliquots were stored at -80 °C.

Statistical Analysis. The data are expressed as the mean \pm SD of the indicated number of independently performed experiments. Statistical significance ($p < 0.05$) was assessed using Student's *t* test or one-way analysis of variance (ANOVA) coupled with Dunnett's *t* test.

■ ASSOCIATED CONTENT

S Supporting Information

The Supporting Information is available free of charge on the ACS Publications website at DOI: [10.1021/acs.jmedchem.5b00764](https://doi.org/10.1021/acs.jmedchem.5b00764).

Synthetic procedures and spectroscopic data for **(±)-5b**, **(±)-12b**, and **13–15**, HPLC analysis of biologically tested compounds, and antitumor activity of *(R)*-cryptopleurine (2) (PDF)

Molecular formula strings (CSV)

■ AUTHOR INFORMATION

Corresponding Authors

*S.K.L.: phone, +82-2-880-2475; e-mail, sklee61@snu.ac.kr.

*S.K.: phone, +82-2-880-2487; e-mail, pennkim@snu.ac.kr.

Author Contributions

Y.K. and J.S. contributed equally to this work. All authors have given approval to the final version of the manuscript.

Notes

The authors declare no competing financial interest.

■ ACKNOWLEDGMENTS

This work was supported by the SRC/ERC program (Grant R-11-2007-107-02001-0), MRC program (Grant 2009-0083533), and Basic Science Research Program (Grant NRF-2014R1A4A1007304) of the National Research Foundation of Korea (NRF) funded by the Korea government (MSIP). This work was also supported by NRF grant funded by the Korea government (NRF-2012-Fostering Core Leaders of the Future Basic Science Program).

■ ABBREVIATIONS USED

AP1, activator protein 1; CRE, cAMP response element; DMEM, Dulbecco's modified Eagle medium; EDCI, N-ethyl-N'-(3-dimethylaminopropyl)carbodiimide hydrochloride; EMT, epithelial-mesenchymal transition; FBS, fetal bovine serum; JNK, c-Jun N-terminal protein kinase; NNMT, nicotinamide N-methyltransferase; PCNA, proliferating cell nuclear antigen; PIFA, phenyliodine(III) bis(trifluoroacetate); RIPA, radioimmunoprecipitation assay; RPMI, Roswell Park Memorial Institute; siRNA, small interfering RNA; SRB, sulforhodamine B; uPA, urokinase-type plasminogen activator

■ REFERENCES

(1) For selected reviews, see the following: (a) Newman, D. J.; Cragg, G. M. Natural Products As Sources of New Drugs over the 30 Years from 1981 to 2010. *J. Nat. Prod.* **2012**, *75*, 311–335. (b) Mishra, B. B.; Tiwari, V. K. Natural products: An evolving role in future drug discovery. *Eur. J. Med. Chem.* **2011**, *46*, 4769–4807. (c) Cragg, G. M.; Grothaus, P. G.; Newman, D. J. Impact of Natural Products on Developing New Anti-Cancer Agents. *Chem. Rev.* **2009**, *109*, 3012–3043. (d) Harvey, A. L. Natural products in drug discovery. *Drug Discovery Today* **2008**, *13*, 894–901. (e) Butler, M. S. Natural products to drugs: natural product-derived compounds in clinical trials. *Nat. Prod. Rep.* **2008**, *25*, 475–516.

(2) (a) Larsson, J.; Gottfries, J.; Muresan, S.; Backlund, A. ChemGPS-NP: Tuned for Navigation in Biologically Relevant Chemical Space. *J. Nat. Prod.* **2007**, *70*, 789–794. (b) Nören-Müller, A.; Reis-Correa, I.; Prinz, H.; Rosenbaum, C.; Saxena, K.; Schwalbe, H.; Vestweber, D.; Cagna, G.; Schunk, S.; Schwarz, O.; Schiewe, H.; Waldmann, H. Discovery of protein phosphatase inhibitor classes by biology-oriented synthesis. *Proc. Natl. Acad. Sci. U. S. A.* **2006**, *103*, 10606–10611. (c) Koch, M. A.; Schuffenhauer, A.; Scheck, M.; Wetzel, S.; Casaulta, M.; Odermatt, A.; Ertl, P.; Waldmann, H. Charting biologically relevant chemical space: A structural classification of natural products (SCONP). *Proc. Natl. Acad. Sci. U. S. A.* **2005**, *102*, 17272–17277. (d) Koch, M. A.; Wittenberg, L.-O.; Basu, S.; Jeyaraj, D. A.; Gourzoulidou, E.; Reinecke, K.; Odermatt, A.; Waldmann, H. Compound library development guided by protein structure similarity clustering and natural product structure. *Proc. Natl. Acad. Sci. U. S. A.* **2004**, *101*, 16721–16726.

(3) For reviews, see the following: (a) Burtoloso, A. C. B.; Bertonha, A. F.; Rosset, I. G. Synthesis of Alkaloids: Recent Advances in the Synthesis of Phenanthroindolizidine Alkaloids. *Curr. Top. Med. Chem.* **2014**, *14*, 191–199. (b) Chemler, S. R. Phenanthroindolizidines and Phenanthroquinolizidines: Promising Alkaloids for Anti-Cancer Therapy. *Curr. Bioact. Compd.* **2009**, *5*, 2–19. (c) Li, Z.; Jin, Z.; Huang, R. Isolation, Total Synthesis and Biological Activity of Phenanthroindolizidine and Phenanthroquinolizidine Alkaloids. *Synthesis* **2001**, No. 16, 2365–2378. (d) Gellert, E. The Indolizidine Alkaloids. *J. Nat. Prod.* **1982**, *45*, 50–73.

(4) NCI 60-cell assay results, along with in vivo data, are available at [http://ntp.nci.nih.gov/dtpstandard/dwindex/index.jsp](http://.dtp.nci.nih.gov/dtpstandard/dwindex/index.jsp).

(5) (a) Suffness, M.; Douros, J. In *Anticancer Agents Based on Natural Product Models*; Cassady, J. M., Douros, J. D., Eds.; Academic Press: London, 1980; pp 465–487. (b) Gopalakrishnan, C.; Shankaranarayanan, D.; Kameswaran, L.; Natarajan, S. Pharmacological investigations of tylophorine, the major alkaloid of *Tylophora indica*. *Indian J. Med. Res.* **1979**, *69*, 513–520. (c) Goldin, A.; Serpick, A. A.; Mantel, N. Experimental screening procedures and clinical predictability value. *Cancer Chemother. Rep.* **1966**, *50*, 173–218.

(6) (a) Fu, Y.; Lee, S. K.; Min, H.-Y.; Lee, T.; Lee, J.; Cheng, M.; Kim, S. Synthesis and structure-activity studies of antofine analogues as potential anticancer agents. *Bioorg. Med. Chem. Lett.* **2007**, *17*, 97–100. (b) Wang, K.; Wang, W.; Wang, Q.; Huang, R. Efficient Synthesis of Aza-Phenanthroindolizidine and Aza-Phenanthroquinolizidine and Anticancer Activities. *Lett. Org. Chem.* **2008**, *5*, 383–390.

- (7) Huang, M.-T.; Grossman, A. P. Mode of Action of Tylocrebrine: Effects on Protein and Nucleic Acid Synthesis. *Mol. Pharmacol.* **1972**, *8*, 538–550.
- (8) (a) Rao, K. N.; Venkatachalam, S. R. Inhibition of dihydrofolate reductase and cell growth activity by the phenanthroindolizidine alkaloids pergularanine and tylophorinidine: the in vitro cytotoxicity of these plant alkaloids and their potential as antimicrobial and anticancer agents. *Toxicol. In Vitro* **2000**, *14*, 53–59. (b) Rao, K. N.; Bhattacharya, R. K.; Venkatachalam, S. R. Inhibition of thymidylate synthase and cell growth by the phenanthroindolizidine alkaloids pergularanine and tylophorinidine. *Chem.-Biol. Interact.* **1997**, *106*, 201–212.
- (9) Gao, W.; Lam, W.; Zhong, S.; Kaczmarek, C.; Baker, D. C.; Cheng, Y.-C. Novel Mode of Action of Tylophorine Analogs as Antitumor Compounds. *Cancer Res.* **2004**, *64*, 678–688.
- (10) (a) Song, J.; Kwon, Y.; Kim, S.; Lee, S. K. Antitumor Activity of Phenanthroindolizidine Alkaloids Is Associated with Negative Regulation of Met Endosomal Signaling in Renal Cancer Cells. *Chem. Biol.* **2015**, *22*, 504–515. (b) Qiu, Y.-Q.; Yang, C.-W.; Lee, Y.-Z.; Yang, R.-B.; Lee, C.-H.; Hsu, H.-Y.; Chang, C.-C.; Lee, S.-J. Targeting a ribonucleoprotein complex containing the caprin-1 protein and the c-Myc mRNA suppresses tumor growth in mice: an identification of a novel. *oncotarget.* **2015**, *6*, 2148–2163. (c) Chen, C.-Y.; Yang, S.-C.; Lee, K.-H.; Yang, X.; Wei, L.-Y.; Chow, L.-P.; Wang, T.-C. V.; Hong, T.-M.; Lin, J.-C.; Kuan, C.; Yang, P.-C. The Antitumor Agent PBT-1 Directly Targets HSP90 and hnRNP A2/B1 and Inhibits Lung Adenocarcinoma Growth and Metastasis. *J. Med. Chem.* **2014**, *57*, 677–685. (d) Lai, C.-Y.; Pan, S.-L.; Yang, X.-M.; Chang, L.-H.; Chang, Y.-L.; Yang, P.-C.; Lee, K.-H.; Teng, C.-M. Depletion of 4E-BP1 and regulation of autophagy lead to YXM110-induced anticancer effects. *Carcinogenesis* **2013**, *34*, 2050–2060. (e) Yang, C.-W.; Lee, Y.-Z.; Hsu, H.-Y.; Wu, C.-M.; Chang, H.-Y.; Chao, Y.-S.; Lee, S.-J. c-Jun-mediated anticancer mechanisms of tylophorine. *Carcinogenesis* **2013**, *34*, 1304–1314. (f) Min, H. Y.; Chung, H. J.; Kim, E. H.; Kim, S.; Park, E. J.; Lee, S. K. Inhibition of cell growth and potentiation of tumor necrosis factor-alpha (TNF- α)-induced apoptosis by a phenanthroindolizidine alkaloid antofine in human colon cancer cells. *Biochem. Pharmacol.* **2010**, *80*, 1356–1364.
- (11) For selected examples, see the following: (a) Miguélez, J.; Boto, A.; Marín, R.; Díaz, M. Simplification of antitumoral phenanthroindolizidine alkaloids: Short synthesis of cytotoxic indolizidinone and pyrrolidine analogs. *Eur. J. Med. Chem.* **2013**, *66*, 540–554. (b) Yang, X.; Shi, Q.; Lai, C.-Y.; Chen, C.-Y.; Ohkoshi, E.; Yang, S.-C.; Wang, C.-Y.; Bastow, K. F.; Wu, T.-S.; Pan, S.-L.; Teng, C.-M.; Yang, P.-C.; Lee, K.-H. Antitumor Agents 295. E-Ring Hydroxylated Antofine and Cryptopleurine Analogues as Antiproliferative Agents: Design, Synthesis, and Mechanistic Studies. *J. Med. Chem.* **2012**, *55*, 6751–6761. (c) Lee, Y.-Z.; Yang, C.-W.; Hsu, H.-Y.; Qiu, Y.-Q.; Yeh, T.-K.; Chang, H.-Y.; Chao, Y.-S.; Lee, S.-J. Synthesis and Biological Evaluation of Tylophorine-Derived Dibenzozquinolines as Orally Active Agents: Exploration of the Role of Tylophorine E Ring on Biological Activity. *J. Med. Chem.* **2012**, *55*, 10363–10377. (d) Yang, X.; Shi, Q.; Yang, S.-C.; Chen, C.-Y.; Yu, S.-L.; Bastow, K. F.; Morris-Natschke, S. L.; Wu, P.-C.; Lai, C.-Y.; Wu, T.-S.; Pan, S.-L.; Teng, C.-M.; Lin, J.-C.; Yang, P.-C.; Lee, K.-H. Antitumor Agents 288: Design, Synthesis, SAR, and Biological Studies of Novel Heteroatom-Incorporated Antofine and Cryptopleurine Analogues as Potent and Selective Antitumor Agents. *J. Med. Chem.* **2011**, *54*, 5097–5107. (e) Ikeda, T.; Yaegashi, T.; Matsuzaki, T.; Yamazaki, R.; Hashimoto, S.; Sawada, S. Synthesis of phenanthroindolizidine alkaloids and evaluation of their antitumor activities and toxicities. *Bioorg. Med. Chem. Lett.* **2011**, *21*, 5978–5981. (f) Yang, X.; Shi, Q.; Liu, Y.-N.; Zhao, G.; Bastow, K. F.; Lin, J.-C.; Yang, S.-C.; Yang, P.-C.; Lee, K.-H. Antitumor Agents 268. Design, Synthesis, and Mechanistic Studies of New 9-Substituted Phenanthrene-Based Tylophorine Analogues as Potent Cytotoxic Agents. *J. Med. Chem.* **2009**, *52*, 5262–5268. (g) Su, C.-R.; Damu, A. G.; Chiang, P.-C.; Bastow, K. F.; Morris-Natschke, S. L.; Lee, K.-H.; Wu, T.-S. Total synthesis of phenanthroindolizidine alkaloids (\pm)-antofine, and their dehydro congeners and evaluation of their cytotoxic activity. *Bioorg. Med. Chem.* **2008**, *16*, 6233–6241. (12) Kwon, Y.; Song, J.; Lee, B.; In, J.; Song, H.; Chung, H.-J.; Lee, S. K.; Kim, S. Design, synthesis, and evaluation of a water-soluble antofine analogue with high antiproliferative and antitumor activity. *Bioorg. Med. Chem.* **2013**, *21*, 1006–1017. (13) AlogP, PSA, logBB, and solubility values were calculated using Bovia/ADME prediction software. (14) Lipinski, C. A.; Lombardo, F.; Dominy, B. W.; Feeney, P. J. Experimental and computational approaches to estimate solubility and permeability in drug discovery and development settings. *Adv. Drug Delivery Rev.* **1997**, *23*, 3–25. (15) Fürstner, A.; Kennedy, J. W. J. Total Syntheses of the Tylophora Alkaloids Cryptopleurine, ($-$)-Antofine, ($-$)-Tylophorine, and ($-$)-Ficuseptine C. *Chem. - Eur. J.* **2006**, *12*, 7398–7410. (16) (a) Chausset-Boissarie, L.; Arvai, R.; Cumming, G. R.; Guenee, L.; Kundig, E. P. Asymmetric synthesis of (+)-vertine and (+)-lythrine. *Org. Biomol. Chem.* **2012**, *10*, 6473–6479. (b) The enantiomeric excess was determined by chiral HPLC analysis of (R)-N-Cbz-piperidineethanol prepared from a small amount of salt. (17) (a) Kita, Y.; Gyoten, M.; Ohtsubo, M.; Tohma, H.; Takada, T. Non-phenolic oxidative coupling of phenol ether derivatives using phenyliodine(III) bis(trifluoroacetate). *Chem. Commun.* **1996**, 1481–1482. (b) Moreno, I.; Tellitu, I.; Domínguez, E.; SanMartín, R. A Simple Route to New Phenanthro- and Phenanthroid-Fused Thiazoles by a PIFA-Mediated (Hetero)biaryl Coupling Reaction. *Eur. J. Org. Chem.* **2002**, *2002*, 2126–2135. (18) (a) Liéby-Muller, F.; Marion, F.; Schmitt, P.; Annereau, J.-P.; Kruczynski, A.; Guilbaud, N.; Bailly, C. Synthesis and biological evaluation of ($-$)-6-O-desmethylcryptopleurine and analogs. *Bioorg. Med. Chem. Lett.* **2015**, *25*, 184–187. (b) Yang, X.; Shi, Q.; Bastow, K. F.; Lee, K.-H. Antitumor Agents. 274. A New Synthetic Strategy for E-Ring SAR Study of Antofine and Cryptopleurine Analogues. *Org. Lett.* **2010**, *12*, 1416–1419. (19) A recent report showed that the substitution of the C-6 methoxy group of cryptopleurine with a hydroxyl group led to similar antiproliferative activity. See ref 18a. (20) See the Supporting Information for synthetic details. (21) Goepel, M.; Rübben, H. Adjuvant therapy in renal cancer. *World J. Urol.* **1991**, *9*, 232–236. (22) Shapiro, G. I. Cyclin-dependent kinase pathways as targets for cancer treatment. *J. Clin. Oncol.* **2006**, *24*, 1770–1783. (23) Mancini, V.; Battaglia, M.; Ditonno, P.; Palazzo, S.; Lastilla, G.; Montironi, R.; Bettocchi, C.; Cavalcanti, E.; Ranieri, E.; Selvaggi, F. P. Current Insights in Renal Cell Cancer Pathology. *Urol. Oncol.: Semin. Orig. Invest.* **2008**, *26*, 225–238. (24) (a) Roeßler, M.; Rollinger, W.; Palme, S.; Hagmann, M.-L.; Berndt, P.; Engel, A. M.; Schneidinger, B.; Pfeffer, M.; Andres, H.; Karl, J. Identification of nicotinamide N-methyltransferase as a novel serum tumor marker for colorectal cancer. *Clin. Cancer Res.* **2005**, *11*, 6550–6557. (b) Xu, J.; Moatamed, F.; Caldwell, J. S.; Walker, J. R.; Kraiem, Z.; Taki, K.; Brent, G. A.; Hershman, J. M. Enhanced expression of nicotinamide N-methyltransferase in human papillary thyroid carcinoma cells. *J. Clin. Endocrinol. Metab.* **2003**, *88*, 4990–4996. (c) Lim, B.; Cho, B.; Kim, Y. N.; Kim, J. W.; Park, S.; Lee, C. Overexpression of nicotinamide N-methyltransferase in gastric cancer tissues and its potential post-translational modification. *Exp. Mol. Med.* **2006**, *38*, 455. (d) Sartini, D.; Santarelli, A.; Rossi, V.; Goteri, G.; Rubini, C.; Ciavarella, D.; Muzio, L. L.; Emanuelli, M. Nicotinamide N-methyltransferase upregulation inversely correlates with lymph node metastasis in oral squamous cell carcinoma. *Mol. Med.* **2007**, *13*, 415–421. (e) Kim, J.; Hong, S. J.; Lim, E. K.; Yu, Y.-S.; Kim, S. W.; Roh, J. H.; Do, I.-G.; Joh, J.-W.; Kim, D. S. Expression of nicotinamide N-methyltransferase in hepatocellular carcinoma is associated with poor prognosis. *J. Exp. Clin. Cancer Res.* **2009**, *28*, 20. (f) Wu, Y.; Siadaty, M.; Berens, M.; Hampton, G.; Theodorescu, D. Overlapping gene expression profiles of cell migration and tumor invasion in human bladder cancer identify metallothionein 1E and nicotinamide N-methyltransferase as novel regulators of cell migration. *Oncogene* **2008**,

27, 6679–6689. (g) Rogers, C. D.; Fukushima, N.; Sato, N.; Shi, C.; Prasad, N.; Hustinx, S. R.; Matsubayashi, H.; Canto, M.; Eshleman, J. R.; Hruban, R. H. Differentiating Pancreatic Lesions by Microarray and QPCR Analysis of Pancreatic Juice RNAs. *Cancer Biol. Ther.* **2006**, *5*, 1383–1389.

(25) (a) Yao, M.; Tabuchi, H.; Nagashima, Y.; Baba, M.; Nakagawa, N.; Ishiguro, H.; Hamada, K.; Inayama, Y.; Kishida, T.; Hattori, K. Gene expression analysis of renal carcinoma: adipose differentiation-related protein as a potential diagnostic and prognostic biomarker for clear-cell renal carcinoma. *J. Pathol.* **2005**, *205*, 377–387. (b) Zhang, J.; Xie, X.-y.; Yang, S.-w.; Wang, J.; He, C. Nicotinamide N-methyltransferase protein expression in renal cell cancer. *J. Zhejiang Univ., Sci., B* **2010**, *11*, 136–143. (c) Sartini, D.; Muzzonigro, G.; Milanese, G.; Pierella, F.; Rossi, V.; Emanuelli, M. Identification of nicotinamide N-methyltransferase as a novel tumor marker for renal clear cell carcinoma. *J. Urol.* **2006**, *176*, 2248–2254.

(26) (a) Sartini, D.; Seta, R.; Pozzi, V.; Morganti, S.; Rubini, C.; Zizzi, A.; Tomasetti, M.; Santarelli, L.; Emanuelli, M. Role of nicotinamide N-methyltransferase in nonsmall cell lung cancer: in vitro effect of shRNA-mediated gene silencing on tumorigenicity. *Biol. Chem.* **2015**, *396*, 225–234. (b) Xie, X.; Yu, H.; Wang, Y.; Zhou, Y.; Li, G.; Ruan, Z.; Li, F.; Wang, X.; Liu, H.; Zhang, J. Nicotinamide N-methyltransferase enhances the capacity of tumorigenesis associated with the promotion of cell cycle progression in human colorectal cancer cells. *Arch. Biochem. Biophys.* **2014**, *564*, 52–66. (c) Pozzi, V.; Sartini, D.; Morganti, S.; Giuliante, R.; Di Ruscio, G.; Santarelli, A.; Rocchetti, R.; Rubini, C.; Tomasetti, M.; Giannatempo, G.; Orlando, F.; Provinciali, M.; Lo Muzio, L.; Emanuelli, M. RNA-mediated gene silencing of nicotinamide N-methyltransferase is associated with decreased tumorigenicity in human oral carcinoma cells. *PLoS One* **2013**, *8*, e71272.

(27) (a) Dolado, I.; Nebreda, A. R. Regulation of tumorigenesis by p38 α MAP kinase. In *Stress-Activated Protein Kinases*; Springer: Berlin, 2008; pp 99–128. (b) Hipp, S.; Berg, D.; Ergin, B.; Schuster, T.; Hapfelmeier, A.; Walch, A.; Avril, S.; Schmalfeldt, B.; Höfler, H.; Becker, K.-F. Interaction of Snail and p38 mitogen-activated protein kinase results in shorter overall survival of ovarian cancer patients. *Virchows Arch.* **2010**, *457*, 705–713. (c) Zohn, I. E.; Li, Y.; Skolnik, E. Y.; Anderson, K. V.; Han, J.; Niswander, L. p38 and a p38-interacting protein are critical for downregulation of E-cadherin during mouse gastrulation. *Cell* **2006**, *125*, 957–969. (d) Huang, S.; New, L.; Pan, Z.; Han, J.; Nemerow, G. R. Urokinase plasminogen activator/urokinase-specific surface receptor expression and matrix invasion by breast cancer cells requires constitutive p38alpha mitogen-activated protein kinase activity. *J. Biol. Chem.* **2000**, *275*, 12266–12272.

(28) Rousseau, S.; Dolado, I.; Beardmore, V.; Shapiro, N.; Marquez, R.; Nebreda, A. R.; Arthur, J. S.; Case, L. M.; Tessier-Lavigne, M.; Gaestel, M.; Cuenda, A.; Cohen, P. CXCL12 and CSa trigger cell migration via a PAK1/2-p38alpha MAPK-MAPKAP-K2-HSP27 pathway. *Cell. Signalling* **2006**, *18*, 1897–1905.

(29) Avdeef, A.; Testa, B. Physicochemical profiling in drug research: a brief survey of the state-of-the-art of experimental techniques. *Cell. Mol. Life Sci.* **2002**, *59*, 1681–1689.

(30) (a) In the (R)-cryptopleurine-treated group, the body weights were significantly reduced compared with the control group. (b) See the [Supporting Information](#) for details..